UNIVERSIDADE FEDERAL DE JUIZ DE FORA

ENGENHARIA ELÉTRICA

PROGRAMA DE PÓS-GRADUAÇÃO EM ENGENHARIA ELÉTRICA

Wesley Mateus Cantarino

Measurement and Characterization of Multiconductor Cables in Railway Signaling Systems

Juiz de Fora

2025

Wesley Mateus Cantarino

Measurement and Characterization of Multiconductor Cables in Railway Signaling Systems

Dissertação apresentada ao Programa de Pós-Graduação em Engenharia Elétrica da Universidade Federal de Juiz de Fora como requisito parcial à obtenção do título de Mestre em Engenharia Elétrica. Área de concentração: Sistemas Eletrônicos.

Orientador: Prof. Dr. Moisés Vidal Ribeiro

Coorientador: Prof. Dr. Luciano Manhães de Andrade Filho

Coorientador: Prof. Dr. Andrea M. Tonello

Juiz de Fora

2025

Ficha catalográfica elaborada através do Modelo Latex do CDC da UFJF com os dados fornecidos pelo(a) autor(a)

Mateus Cantarino, Wesley.
Measurement and Characterization of Multiconductor Cables in Railway Signaling Systems / Wesley Mateus Cantarino. – 2025.
63 f. : il.

Orientador: Prof. Dr. Moisés Vidal Ribeiro
Coorientador: Prof. Dr. Luciano Manhães de Andrade Filho
Coorientador: Prof. Dr. Andrea M. Tonello
Dissertação (Mestrado) – Universidade Federal de Juiz de Fora, Engenharia Elétrica. Programa de Pós-Graduação em Engenharia Elétrica, 2025.

1. (sistema de sinalização ferroviária). 2. (linha de transmissão para multicondutores). 3. (impedância característica). 4. (parâmetros de espalhamento). 5. (diafonia). 6. (ruído adtivo) I. Ribeiro, Moisés Vidal, orient. II. Filho, Luciano Manhães de Andrade, coorient. III. Tonello, Andrea M., coorient. IV. Título.

Wesley Mateus Cantarino

Measurement and Characterization of Multiconductor Cables in Railway Signaling Systems

Dissertação apresentada ao Programa de Pós-Graduação em Engenharia Elétrica da Universidade Federal de Juiz de Fora como requisito parcial à obtenção do título de Mestre em Engenharia Elétrica. Área de concentração: Sistemas Eletrônicos.

Aprovada em: 21 de Agosto de 2025

FEDERAL UNIVERSITY OF JUIZ DE FORA
RESEARCH AND GRADUATE PROGRAMS OFFICE

Wesley Mateus Cantarino

Measurement and Characterization of Multiconductor Cables in Railway Signaling Systems

Dissertation submitted to the Graduate Program in Electrical Engineering of the Federal University of Juiz de Fora as a partial requirement for obtaining a Master's degree in Electrical Engineering.
Concentration area: Electronic Systems

Approved on 21 of August of 2025.

EXAMINING BOARD

Prof. Dr. Moisés Vidal Ribeiro – Academic Advisor
Federal University of Juiz de Fora

Prof. Dr. Luciano Manhães de Andrade Filho – Academic Co-Advisor
Federal University of Juiz de Fora

Prof. Dr. Andrea M. Tonello – Academic Co-Advisor
Klagenfurt University

Prof. Dr. Alberto Resende de Conti
Federal University of Minas Gerais

Prof. Dr. Leandro Ramos de Araujo
Federal University of Juiz de Fora

Juiz de Fora, 08/21/2025.

To my family
To my friends
To my advisors
To my colleagues

ACKNOWLEDGMENTS

Agradeço primeiramente a Deus por ter me conduzido e cuidado de mim.

Agradeço à minha família, especialmente à minha mãe, Creusa Aparecida de Campos Cantarino, ao meu pai, Beijamim Valério Cantarino, e à minha noiva Deiziele Dornelas Couto, por todo o apoio que me deram ao longo desses anos de vida.

Gostaria de agradecer também aos meus amigos e colegas que fiz durante minha vida acadêmica, com os quais compartilhei as alegrias e dificuldades da pós-graduação. Agradeço também aos meus colegas do Laboratório de Comunicações (LCom) pela atenção e disposição em ajudar durante todo o percurso do mestrado.

Agradeço também ao meu orientador, Prof. Dr. Moisés Vidal Ribeiro, e ao meus coorientadores, Prof. Dr. Luciano Manhães de Andrade Filho e Prof. Dr. Andrea M. Tonello, pela orientação e dicas recebidas. Agradeço também ao Dr. Luís Guilherme da Silva, pela orientação e ajuda desde a minha primeira bolsa de iniciação científica até o mestrado. Sou grato também à banca examinadora, por aceitar avaliar este trabalho e contribuir com sugestões e comentários.

Finalmente, expresso minha gratidão a todos os docentes e colaboradores da Universidade Federal de Juiz de Fora por seu apoio e contribuição para minha educação acadêmica e desenvolvimento profissional.

"O assunto mais importante do mundo pode ser simplificado até ao ponto em que todos possam apreciá-lo e compreendê-lo. Isso é - ou deveria ser - a mais elevada forma de arte."

Charles Chaplin (1889-1977)

RESUMO

Esta dissertação discute a medição e caracterização de cabos multicondutores usados em sistemas de sinalização ferroviária. Ao aplicar a teoria de linha de transmissão para multicondutores, na configuração de n fios, o presente trabalho faz uso de um formalismo matemático para modelar o comportamento dos cabos multicondutores utilizados em sistemas de sinalização ferroviária e, consequentemente, realizar análises a partir de simulações numéricas. Visando promover a caracterização desses condutores, a presente dissertação discute três arranjos experimentais para a realização de campanhas de medição em laboratório e no campo. Os arranjos experimentais contemplam a medição da impedância característica, parâmetros de espalhamento, resposta em frequência de diafonia e ruído aditivo na faixa de frequência entre 20 Hz-2 MHz. A seguir, a presente dissertação descreve as campanhas de medição realizadas em laboratório e no campo. A discussão comparativa entre os resultados coletados a partir das simulações numéricas baseadas na modelagem adotada e através das campanhas de medição no laboratório e no campo apresentam elevado nível de concordância. Finalmente, uma análise da densidade espectral de potência do ruído aditivo, juntamente com a magnitude da resposta de frequência de um condutor no cabo multicondutor empregado em sinalização ferroviária, confirma que tanto a comunicação de dados quanto o sensoriamento podem ser realizados, com certas restrições, a partir do emprego de sinais elétricos de baixa potência, um requisito essencial para evitar interferência nos sistemas de sinalização ferroviária existentes.

Palavras-chave: sistema de sinalização ferroviária, linha de transmissão para multicondutores, impedância característica, parâmetros de espalhamento, diafonia, ruído aditivo.

ABSTRACT

This thesis presents the measurement and characterization of multiconductor cables used in railway signaling systems. By applying multiconductor transmission line theory to an n-wire configuration, this work applies a mathematical formalism for analyzing the behavior of these multiconductor cables through numerical simulations. Aiming to provide a characterization of these cables, this thesis discusses three experimental setups for conducting measurement campaigns both in the laboratory and in the field. These setups cover the measurement of characteristic impedance, scattering parameters, crosstalk frequency response, and additive noise over the frequency range from 20 Hz-2 MHz. The dissertation then describes the measurement campaigns performed in both environments. A comparative discussion between results obtained from the simulations based on the adopted model and those from the laboratory and field campaigns shows a high level of agreement. Finally, an analysis of the additive noise power spectral density, together with the magnitude of the frequency response of a single conductor within the multiconductor cable used in railway signaling, confirms that both data communication and sensing can be carried out under certain constraints using low-power electrical signals. The use of low-power electrical signals is an essential requirement to avoid interference with legacy railway signaling systems.

Keywords: railway signaling system, multiconductor cable, characteristic impedance, scattering parameters, crosstalk, additive noise.

LIST OF FIGURES

LIST OF TABLES

LIST OF ACRONYMS

AC	alternating current
BNC	bayonet neill–concelman
CI	integrated circuit
DC	direct current
DUT	device under test
EMI	Electromagnetic Interference
FDR	frequency-domain reflectometry
FEXT	far-end crosstalk
IoT	Internet of Things
LISN	line impedance stabilization network
LCom	Communications Laboratory
ML	machine learning
MTL	multiconductor transmission lines
MIMO	multiple-input multiple-output
NEXT	near-end crosstalk
PCB	printed circuit board
PNL35	2035 National Logistics Plan
PNL50	2050 National Logistics Plan
PLC	power line communication
PSD	power spectral density
p.u.l.	per-unit-length
SCU	signal conditioning unit
SPD	surge protection devices
TEM	transverse electromagnetic mode
TDR	time-domain reflectometry

Tx	transmitter
UPS	uninterruptible power supply
UFJF	Federal University of Juiz de Fora
UV	ultraviolet
Rx	receiver
VNA	vector network analyser

CONTENTS

1 INTRODUCTION

The expansion of railway transportation systems has been recognized as a relevant decarbonization action to mitigate the climate emergency and promote sustainable development in the land transportation sector. Indeed, railways are well-established as the most efficient land transportation systems for a large number of cargo and people, especially when distances increase compared to roads. Although the advantages of a robust railway system are evident for a continental country like Brazil, decades of insufficient long-term planning, ineffective decision-making, and weak governance have eroded its operational efficiency [1].

According to the National Association of Railway Transporters (in Portuguese, Associação Nacional dos Transportadores Ferroviários – ANTF) [2], there are more than $31,000$ km of railways in Brazil, which is insufficient to promote efficiency in the Brazilian transportation systems. Currently, the existing Brazilian railway transportation system is primarily used for mining and agriculture, as well as the steel and cement industries, civil construction, and oil production. Additionally, a few Brazilian cities have urban railway systems for public transportation, indicating that Brazil is lagging in meeting its transportation efficiency needs.

It is important to mention that Brazil has undergone significant transformations in its railway sector, particularly with privatization efforts in the 1990s, which resulted in notable improvements in safety and freight capacity [1, 3]. These reforms have strengthened the role of railways in supporting the country's growing demand for efficient transport of goods, especially in sectors such as mining, agriculture, steel and cement industries, civil construction, and oil, where long-distance logistics are crucial to economic success. On the other hand, privatization did not address network expansion, which is a crucial issue for a country with a railway network density of only 3.6 km/1000km^2 and very low compared to countries such as the United States of America, China, India, and Europe, see details in Table 1.

The railway transportation system remains relatively underdeveloped compared to the roadway network in Brazil. Currently, Brazil is relying on 2035 National Logistics Plan (PNL35) to expand its railway network up to 2035. The PNL35 is a strategic document from the Brazilian government, outlining an action plan for the development of

Tabela 1 – Railway Network Density Comparison

Region	Area (km^2)	Railway Network (km)	Railway Network Density ($km/1\,000\ km^2$)
Brazil	8,516,000	30,576	3.59
China	9,597,000	155,000	16.15
USA	9,834,000	220,044	22.38
India	3,287,000	68,584	20.87
European Union	4,233,000	200,947	47.47

the country's transportation sector through 2035. It seeks, for the first time, to optimize transport infrastructure by integrating different modes (road, rail, waterway, air, and pipeline) to ensure greater efficiency, safety, and sustainability in the transportation of goods and people. In 2025, the Brazilian government established a new working group to produce the 2050 National Logistics Plan (PNL50), which will focus on the same aims of PNL50 with some updates to expand railway transportation systems up to 2050 [4].

Overall, there are initiatives to modernize the Brazilian railway network [1]; however, much of its infrastructure still depends on legacy technologies installed decades ago, with minimal subsequent upgrades. Exposed to natural weathering—extreme temperatures, humidity, and corrosion [5, 6]—this aging infrastructure suffers physical degradation that undermines component integrity, highlighting the necessity of continuous asset degradation monitoring [7]. Consequently, the railway infrastructure becomes more vulnerable to environmental stressors, the likelihood of service disruptions grows, further complicating railway operations and jeopardizing the safe transport of goods and passengers [8]. Therefore, maintenance operations are often required to minimize the impact of these problems on the railway transportation system. Additionally, it is crucial to develop strategies that reduce train downtime during maintenance activities while minimizing adverse effects on overall railway operations. Predictive and corrective maintenance have been widely applied to maintain the efficiency of railway infrastructure.

In railway transportation systems, both predictive and corrective maintenance are applied to the electrical power, electronics, civil, and rolling-stock subsystems. The electronics subsystem supports traffic control and communications, making it essential that track-circuit signaling be kept in reliable working order to prevent accidents by maintaining safe separation between trains, preventing simultaneous authorization of conflicting routes, and enforcing speed limits through the automatic activation of braking systems when a train exceeds its permitted velocity. One common failure in railway transportation systems is false occupancy, where a track circuit indicates that a section is occupied despite the absence of a train [9]. When the control center detects false occupancy, a maintenance crew must be dispatched to locate and remedy the fault. Depending on the cause and size of the track circuit, this process can be time-consuming, halting traffic on the affected section and resulting in significant economic losses.

Regarding the track circuit, condition monitoring and fault diagnosis of railway signaling cables have garnered significant attention due to their critical role in ensuring the safety and reliability of railway operations. The signaling cables are directly buried, and, consequently, their conditions deteriorate over time, influenced by soil composition and climate factors. This degradation can lead to several undesirable outcomes, including inaccurate train positioning information, delayed signaling, and, in some cases, unsafe operating conditions. If left unchecked, the degradation of signaling cables can remarkably reduce the efficiency of railway operations and increase the risk of accidents [10].

Several studies have proposed advanced methods to assess the health of buried cables. Vijay et al. [11,12] proposed an orthogonal multitone time-domain reflectometry approach for soft fault detection in underground railway cables, leveraging software-defined radios and a Bayesian framework to compute a comprehensive cable health index. Similarly, Smith et al. [13] highlighted the effectiveness of time-domain reflectometry (TDR) in locating intermittent faults in cables, emphasizing its noise immunity and adaptability to complex impedance scenarios. The relevance of reflectometry techniques is further reinforced in the work by Oliveira et al. [14, 15], who applied both TDR and power line communication (PLC) to detect faults in low- and medium-voltage distribution cables.

The use of PLC for condition monitoring has also been extensively studied. For instance, Prasad et al. [16] demonstrated the application of PLC modems to detect short circuits in underground conductors. Benesl et al. [17] explored broadband PLC to assess the technical condition of cables, while Huo et al. [18] proposed a machine learning-based diagnostic framework embedded in PLC modems for remote monitoring of cable aging, showing promising results in terms of robustness under various load and degradation scenarios.

In addition, Grzechca et al. [19] investigated the impact of outer jacket degradation on the communication performance of twisted-pair cables, presenting degradation functions to model environmental effects on cable parameters. Complementing these studies, Oliveira et al. [20] proposed a methodology for estimating frequency responses between cable endpoints, highlighting its value for real-time diagnostics. Recent reviews by Fraga-Lamas et al. [21] and Ribeiro et al. [22] present the evolution of Internet of Things (IoT)-enabled technologies and innovations for predictive maintenance in smart railway systems. Furthermore, Zhuang et al. [23] showed the applicability of IoT-based insulation monitoring in distributed electric power grids, a concept that could be adapted to railway signaling systems.

Overall, the aforementioned studies focus on the use of a specific technique for monitoring the degradation of multiconductor cables that transmit signaling signals between consecutive cabinets housing signaling equipment; however, they do not provide fundamental information about the feasibility of monitoring multiconductor cables based on the use of electrical signals. For instance, the aforementioned studies do not provide information on the useful frequency band and bandwidth for sensing, the characteristic impedance of these cables, or a suitable model for these multiconductor cables.

1.1 OBJECTIVES

Aiming to bridge the aforementioned gap in the literature, this thesis focuses on the measurement and characterization of multiconductor cables used to transmit signaling information in railway signaling systems over the frequency band between 20 Hz and 2 MHz, which can cover both sensing and data communication demands. To achieve this, it discusses measurement setups and campaigns used to obtain a reliable representation of the multiconductor cables employed in railway signaling systems, in terms of scattering parameters, characteristic impedance, and transfer functions. In this sense, the specific objectives are summarized as follows:

- To apply the multiconductor transmission lines (MTL) theory in the frequency domain to model multiconductor cables as n parallel wires, enabling numerical simulations to compute key electrical parameters, including scattering parameters, near-end crosstalk (NEXT) and far-end crosstalk (FEXT) frequency responses, and characteristic impedance.

- To design and implement three experimental setups for measuring scattering parameters, crosstalk (NEXT and FEXT) responses, characteristic impedance, and additive noise in both laboratory and field environments.
- To provide a detailed comparison of the results obtained from numerical simulations and those from laboratory and field measurements, showing the validity of the MTL theory and experimental setups to characterize these multiconductor cables.

1.2 ORGANIZATION

The remainder of this thesis is structured as follows:

- Chapter 2 presents the theoretical basis using MTL theory and formulates the research problem in the context of railway signaling systems.
- Chapter 3 describes the experimental setups developed to measure and characterize multiconductor cables.
- Chapter 4 delineates the laboratory and field measurement campaigns and the data acquisition procedures.
- Chapter 5 analyzes the measured and simulated results, validating the proposed modeling approach.
- Chapter 6 discusses the main contributions of this thesis and proposes directions for future work.

2 FUNDAMENTALS AND PROBLEM FORMULATION

This chapter presents the mathematical model based on the MTL theory [24] in the frequency domain, allowing for deductions of direct, FEXT and NEXT frequency responses that can be used to characterize the multiconductor cables used in railway signaling systems. Moreover, it focuses on the motivations for measuring and characterizing these cables. Finally, it points out the research questions that are addressed in this thesis.

The organization of this chapter is as follows: Section 2.1 discusses the mathematical framework for modeling the cable using MTL theory and Section 2.2 formulates the problem investigated in this thesis.

2.1 MULTICONDUCTOR THEORY

In railway signaling systems, as shown in Fig. 1 (a), metallic cables are employed extensively for the transmission of control and monitoring signals over considerable distances. These cables are generally multiconductor, consisting of multiple insulated conductors arranged in parallel within a shared shielding structure. Railway signaling systems rely on various electronic devices, including relays and actuators, for track circuits. These devices are housed in specialized cabinets to protect them from adverse weather conditions, as shown in Fig. 1 (b). The cabinets are one to three kilometers apart, forming a network interconnected by multiconductor signaling cables. In Brazil, railway signaling systems primarily include uninterruptible power supply (UPS) units, multiconductor cables to connect adjacent cabinets, relays, and lightning protection systems, as specified in [25–27]. Despite their critical role in railway infrastructure, there is a notable lack of modeling efforts specifically dedicated to signaling cables in the context of railway systems. This is in contrast to the extensive literature available in other domains, such as telecommunications, particularly for twisted-pair cables and electric power systems, where multiconductor modeling techniques are well established and widely applied.

In this thesis, the multiconductor cable under study is the WirexControl V70P BFTC - 1 kV model [28]. These signaling cables, with a total diameter of $D = 18.5$ mm,

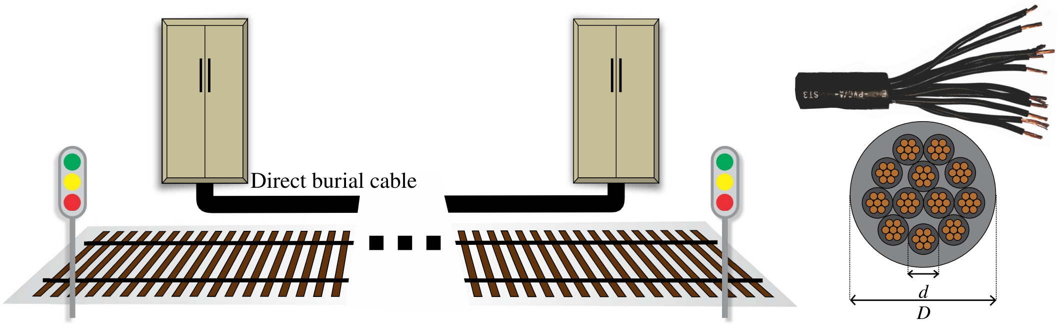

Figura 1 – The railway signaling system: (a) illustration of two cabinets connected through direct burial multiconductor cable, and (b) illustration of multiconductor cable, constituted by 12 conductors, and its cross-section view.

contain 12 conductors each numbered on a printed label starting in 1 to 12, as shown in Fig. 2, each with a diameter of $d = 1.5\,\mathrm{mm}$. The geometry of the cable plays a fundamental role in determining how signals propagate within it. Installed underground along the edge of the railway line, these multiconductor cables must ensure reliable communication for the railway signaling system. Therefore, maintaining the integrity of these signaling cables is crucial to maintaining connectivity between cabinets and ensuring the reliable operation of the railway signaling systems.

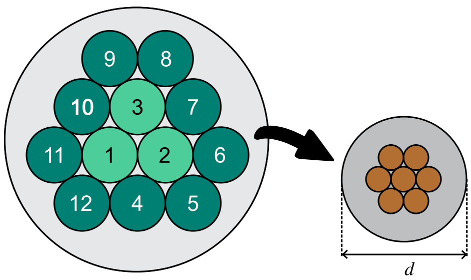

Figura 2 – Cross-section view of the multiconductor cable and the respective label. Note that each conductor consists of 7 copper wires.

A multiconductor cable constituted by n conductors, as illustrated in Fig. 1 (b), can be modeled as n parallel and uniform wires with a reference ground plane. Therefore, Fig. 3 shows a model for n wires arranged parallel along the z-axis with a reference ground plane. This model uses per-unit-length (p.u.l.) equivalent circuit elements. Each conductor has a series resistance (r_{ii}), self and mutual inductance (l_{ij}), capacitance (c_{ij}), and conductance (g_{ij}), reflecting the distributed nature of these parameters along the line, in which $i, j = 1, 2, \cdots, n$. In Fig. 3, the frequency domain representations of the (input) voltages and currents for each ith conductor at distance $z = 0$ (i.e., at the origin) are denoted as $\hat{V}_{0,i}(0)$ and $\hat{I}_{0,i}(0)$, respectively, and at a distance Δz along the transmission line, the (output) voltages and currents are represented by $\hat{V}_{1,i}(\Delta z)$ and $\hat{I}_{1,i}(\Delta z)$, respectively. Assuming a transverse electromagnetic mode (TEM) wave propagating through n wires, the following equations apply [29, 30]:

$$\frac{d}{dz}\hat{\mathbf{V}}_1(z) + \hat{\mathbf{Z}}\hat{\mathbf{I}}_1(z) = 0 \tag{2.1a}$$

$$\frac{d}{dz}\hat{\mathbf{I}}_1(z) + \hat{\mathbf{Y}}\hat{\mathbf{V}}_1(z) = 0, \tag{2.1b}$$

where $\hat{\mathbf{V}}_1(z) = [\hat{V}_{1,1}(z), \hat{V}_{1,2}(z), \cdots, \hat{V}_{1,n}(z)]^{\mathrm{T}}$ and $\hat{\mathbf{I}}_1(z) = [\hat{I}_{1,1}(z), \hat{I}_{1,2}(z), \cdots, \hat{I}_{1,n}(z)]^{\mathrm{T}}$, $\hat{\mathbf{Z}} = \mathbf{R} + j\omega\mathbf{L}$ is the impedance matrix, $\hat{\mathbf{Y}} = \mathbf{G} + j\omega\mathbf{C}$ is the admittance matrix of a z-length segment. The resistance (**R**), inductance (**L**), capacitance (**C**), and conductance (**G**) matrices are also given in p.u.l.. The **R**, **L**, **C**, and **G** matrices are known for each segment, and a few comments on them are as follows:

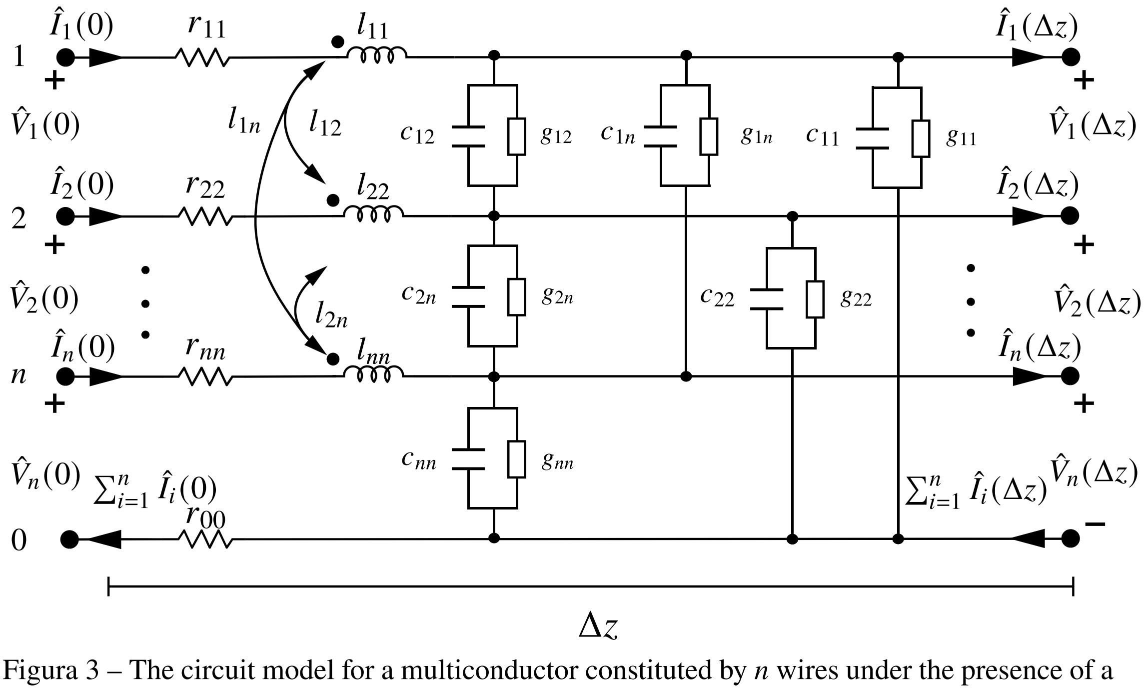

Figura 3 – The circuit model for a multiconductor constituted by n wires under the presence of a ground plane reference.

- **Resistance (R) matrix**: It represents the resistances of all copper conductors, which are denoted by r_{nn}, in a common ground plane with a uniform[1] resistance r_{00}. As the frequency increases, the skin effect intensifies, confining the current to a narrower cross-sectional area of the conductor and consequently leading to a considerable increase in resistance. It is expressed as

$$\mathbf{R} = \begin{bmatrix} r_{00}+r_{11} & r_{00} & \dots & r_{00} \\ r_{00} & r_{00}+r_{22} & \dots & r_{00} \\ \vdots & \vdots & \ddots & \vdots \\ r_{00} & r_{00} & \dots & r_{00}+r_{nn} \end{bmatrix} \Omega/\text{m}. \tag{2.2}$$

- **Inductance (L) matrix**: it comprises the inductance of each conductor and the mutual inductance between the conductors. The geometry of the multiconductor cable and their environment significantly influence these factors. The inductance matrix is given by

$$\mathbf{L} = \begin{bmatrix} l_{11} & l_{12} & \dots & l_{1n} \\ l_{12} & l_{22} & \dots & l_{2n} \\ \vdots & \vdots & \ddots & \vdots \\ l_{1n} & l_{2n} & \dots & l_{nn} \end{bmatrix} \text{H/m}. \tag{2.3}$$

- **Capacitance (C) matrix**: it covers the capacitance between the conductor and the reference plane and the capacitance between the conductors themselves. The capacitance matrix is given by

$$\mathbf{C} = \begin{bmatrix} \sum_{k=1}^{n} c_{1k} & -c_{12} & \dots & -c_{1n} \\ -c_{12} & \sum_{k=1}^{n} c_{2k} & \dots & -c_{2n} \\ \vdots & \vdots & \ddots & \vdots \\ -c_{1n} & -c_{2n} & \dots & \sum_{k=1}^{n} c_{nk} \end{bmatrix} \text{F/m}. \tag{2.4}$$

- **Conductance (G) matrix**: it characterizes the conductive properties of the dielectric material surrounding the conductors. This account for the leakage current between the conductors and the ground plane, which is influenced by the quality

[1] In some cases, it is useful to represent different resistance values, since different cables may exhibit distinct resistance characteristics.

and composition of the dielectric material. The conductance matrix is expressed as

$$\mathbf{G} = \begin{bmatrix} \sum_{k=1}^{n} g_{1k} & -g_{12} & \cdots & -g_{1n} \\ -g_{12} & \sum_{k=1}^{n} g_{2k} & \cdots & -g_{2n} \\ \vdots & \vdots & \ddots & \vdots \\ -g_{1n} & -g_{2n} & \cdots & \sum_{k=1}^{n} g_{nk} \end{bmatrix} \text{S/m}. \tag{2.5}$$

In our context, it is advantageous to represent the MTL as a $2n$-ports network, where each wire represents two ports. It facilitates to measure and calculate the characterization parameters for individual segments and, consequently, the design and analysis by providing a clear framework for understanding signal propagation and crosstalk. Using the $2n$-port network representation, the equations for the k-th cable segment of length Δz is expressed as [31, 32]

$$\begin{bmatrix} \hat{\mathbf{V}}_k(k\Delta z) \\ \hat{\mathbf{I}}_k(k\Delta z) \end{bmatrix} = \hat{\mathbf{\Phi}}_k(\Delta z) \begin{bmatrix} \hat{\mathbf{V}}_{k+1}((k+1)\Delta z) \\ \hat{\mathbf{I}}_{k+1}((k+1)\Delta z) \end{bmatrix}, \tag{2.6}$$

where $k = 0, 1, 2, \cdots, K-1$ and $\hat{\mathbf{\Phi}}_k(\Delta z)$ is the chain parameter matrix for the $(k+1)$-th segment. For the segment between $z = 0$ and $z = \Delta z$, the chain parameter matrix $\hat{\mathbf{\Phi}}_0(\Delta z)$ is given by

$$\begin{aligned} \hat{\mathbf{\Phi}}_0(\Delta z) &= \begin{bmatrix} \mathbf{A}_0 & \mathbf{B}_0 \\ \mathbf{C}_0 & \mathbf{D}_0 \end{bmatrix} \\ &= \begin{bmatrix} \cosh(\gamma\Delta z) & \sinh(\gamma\Delta z)\hat{\mathbf{Z}}_{\text{ca},0} \\ \sinh(\gamma^{\text{T}}\Delta z)\hat{\mathbf{Z}}_{\text{ca},0}^{-1} & \cosh(\gamma^{\text{T}}\Delta z) \end{bmatrix}, \end{aligned} \tag{2.7}$$

where $\hat{\mathbf{Z}}_{\text{ca},0} \in \mathbb{C}^{n\times n}$ is the characteristic impedance matrix in the frequency domain, while the $\gamma \in \mathbb{C}^{n\times n}$ is propagation constant matrix is obtained using [32]

$$\hat{\mathbf{Z}}_{\text{ca},0} = \hat{\mathbf{Z}}\gamma^{-\text{T}} = \hat{\mathbf{Y}}^{-1}\gamma^{\text{T}} \tag{2.8a}$$

$$\gamma^2 = (-\gamma)^2 = \hat{\mathbf{Z}}\hat{\mathbf{Y}}. \tag{2.8b}$$

Based on $\mathbf{Z}_{\text{ca},0}$ and γ, the $\mathbf{R}$, $\mathbf{L}$, $\mathbf{C}$, and $\mathbf{G}$ matrices are given by $\mathbf{R} = \Re\{\gamma Z_{\text{ca},0}\}$, $\mathbf{L} = \frac{1}{\omega}\Im\{\gamma Z_{\text{ca},0}\}$, $\mathbf{C} = \frac{1}{\omega}\Im\{Z_{\text{ca},0}^{-1}\gamma\}$, $\mathbf{G} = \Re\{Z_{\text{ca},0}^{-1}\gamma\}$, respectively, where the symbol $\Re\{.\}$ and $\Im\{.\}$ are operators to extract real and imaginary components, respectively.

Additional details about how to measure the characteristic impedance and the propagation constant for a cable and their implications for cable performance are discussed in Appendix A.

The corresponding scattering parameter matrix for (2.7) is given by

$$\mathbf{S}_0 = \begin{bmatrix} \mathbf{S}_{0,11} & \mathbf{S}_{0,12} \\ \mathbf{S}_{0,21} & \mathbf{S}_{0,22} \end{bmatrix}, \tag{2.9}$$

where $\mathbf{S}_{0,11} = (\mathbf{A}_0 + \mathbf{B}_0\mathbf{Z}_o^{-1} - \mathbf{Z}_o\mathbf{C}_0 - \mathbf{D}_0)(\mathbf{A}_0 + \mathbf{B}_0\mathbf{Z}_o^{-1} + \mathbf{Z}_o\mathbf{C}_0 + \mathbf{D}_0)^{-1}$, $\mathbf{S}_{0,12} = 2(\mathbf{A}_0 + \mathbf{B}_0\mathbf{Z}_o^{-1} + \mathbf{Z}_o\mathbf{C}_0 + \mathbf{D}_0)^{-1}$, $\mathbf{S}_{0,21} = 2(\mathbf{A}_0 + \mathbf{B}_0\mathbf{Z}_o^{-1} + \mathbf{Z}_o\mathbf{C}_0 + \mathbf{D}_0)^{-1}$, and $\mathbf{S}_{0,22} = (-\mathbf{A}_0 + \mathbf{B}_0\mathbf{Z}_o^{-1} - \mathbf{Z}_o\mathbf{C}_0 + \mathbf{D}_0)(\mathbf{A}_0 + \mathbf{B}_0\mathbf{Z}_o^{-1} + \mathbf{Z}_o\mathbf{C}_0 + \mathbf{D}_0)^{-1}$, in which $\mathbf{Z}_o \in \mathbb{C}^{n\times n}$ is the reference impedance. Now, considering $n = 1$ or two-port representation in (2.9) and $Z_{ca,0} \neq Z_o$, in which Z_o is also called the impedance of the port, the scattering matrix is expressed as [33]

$$\mathbf{S}_0 = \begin{bmatrix} S_{0,11} & S_{0,12} \\ S_{0,21} & S_{0,22} \end{bmatrix}, \tag{2.10}$$

$$= \frac{1}{D_s}\begin{bmatrix} (Z_{ca,0}^2 - Z_o^2)\sinh(\gamma L_{ca}) & 2Z_{ca,0}Z_o \\ 2Z_{ca,0}Z_o & (Z_{ca,0}^2 - Z_o^2)\sinh(\gamma L_{ca}) \end{bmatrix}, \tag{2.11}$$

where $D_s = 2Z_{ca,0}Z_o\cosh(\gamma L_{ca}) + (Z_{ca,0}^2 + Z_o^2)\sinh(\gamma L_{ca})$, L_{ca} represents the cable length. In other words, knowning $Z_{ca,0}$, Z_o, γ, and L_{ca} allow us to obtain the scattering parameters. These parameters can be estimated by using a LCR meter.

Relying on the $2n$-port network representation illustrated in Fig. 4, a uniform conductor of length $K\Delta z$ has a chain parameter matrix given by the product of the elementary matrices associated with each segment Δz. This cascading approach guarantees that the overall behavior is accurately represented by the sequential multiplication of these matrices. The chain parameter matrix given by

$$\begin{aligned}\hat{\mathbf{\Phi}}_K(K\Delta z) &= \begin{bmatrix} \mathbf{A}_{K-1} & \mathbf{B}_{K-1} \\ \mathbf{C}_{K-1} & \mathbf{D}_{K-1} \end{bmatrix} \\ &= \prod_{k=0}^{K-1} \hat{\mathbf{\Phi}}_k(\Delta z),\end{aligned} \tag{2.12}$$

from which the scattering matrix $\mathbf{S}_K$ can be obtained. Moreover, from (2.12), the frequency response of an n-wire system can be interpreted as the frequency response of

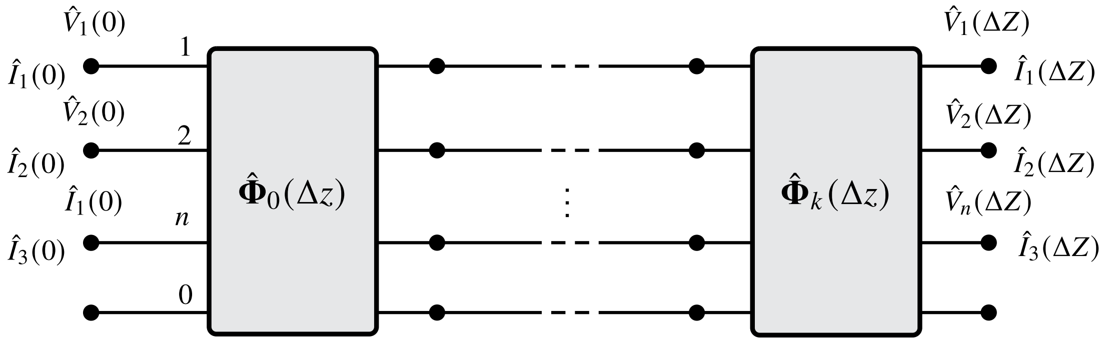

Figura 4 – Cascading of multiple chain parameters for a uniform multiconductor.

a multiple-input multiple-output (MIMO) channel, described by [34]:

$$\hat{\mathbf{V}}(K\Delta z) = \hat{\mathbf{H}}_K(\omega)\hat{\mathbf{V}}(0), \tag{2.13}$$

where $\hat{\mathbf{H}}_K(\omega)$ denotes the voltage transfer function from $z = 0$ to $z = K\Delta z$. The output current is related to the output voltage through the load admittance matrix $\hat{\mathbf{Y}}_\mathrm{L}$ as $\hat{\mathbf{I}}(K\Delta z) = \hat{\mathbf{Y}}_\mathrm{L}\hat{\mathbf{V}}(K\Delta z)$. By applying $\hat{\mathbf{Y}}_\mathrm{L}$ to (2.12), the frequency response matrix $\hat{\mathbf{H}}_K(\omega)$, which characterizes the voltage transfer characteristics of the multiconductor cable, is given by [35]:

$$\hat{\mathbf{H}}_K(\omega) = \left(\mathbf{A}_{K-1} + \mathbf{B}_{K-1}\hat{\mathbf{Y}}_\mathrm{L}\right)^{-1}. \tag{2.14}$$

In the special case where $n = 1$ and $K = 1$, the frequency response $\hat{\mathbf{H}}_1(\omega)$ can be estimated from (2.11), which requires the use of an LCR meter. Alternatively, $\hat{\mathbf{H}}_K(\omega)$ can also be obtained directly by injecting and measuring voltage signals at the terminals of the multiconductor cable.

2.2 PROBLEM FORMULATION

Signaling cables are typically installed using the direct burial method, where they are placed approximately 60 cm below the surface of the ground. This approach is widely employed due to its practicality and cost-effectiveness, offering several notable advantages [11, 12, 36–38]:

- **Economic**: Direct burial is often cost-effective for installing cables because it requires less material (such as conduits) and involves more straightforward installation procedures. Reduces the need for additional protective structures, such as pipes or tubes, making it cheaper than other methods (e.g., installing cables in conduits or tunnels).

- **Technical**: In-place cables are protected from above-ground hazards, such as wind, rain, snow, and physical impact from vehicles or machinery. Being underground also protects them from ultraviolet (UV) radiation, which can degrade exposed cables over time.

However, direct burial of signaling cables presents the following disadvantages [11, 36–39]:

- **Moisture and water ingress**: The threat of moisture and water ingress represents a significant challenge to the reliability of buried cables. The gradual penetration of groundwater, rain, or flooding can compromise the insulation of a cable, particularly if the protective sheath has sustained microscopic damage or failure. This process can lead to chemical degradation of the insulation, reducing its dielectric strength and increasing the risk of short circuits between conductors or to the ground. Over time, continuous exposure to moisture can result in severe operational failures, compromising the overall reliability of the system.
- **Soil composition and corrosiveness**: The composition of the soil surrounding the buried cable has a significant impact on its durability. Certain types of soil, such as acidic or alkaline soils, can accelerate the corrosion of the cable's sheath. Furthermore, the presence of chemicals or salts in the soil, often found in proximity to industrial zones or coastal areas, serves to exacerbate the corrosion process. This deterioration results in a weakening of the mechanical and electrical integrity of the cable, thereby increasing the likelihood of faults.
- **Temperature fluctuations**: Extreme variations in temperature, whether high or low, can cause thermal expansion and contraction of the cable's materials. Over time, this cyclical stress can lead to the formation of cracks or fractures in the insulation and protective layers. In regions with warmer climates, excessive heat may degrade the insulation's material properties, while in colder environments, freezing conditions may exacerbate mechanical vulnerabilities.

- **Rodent and insect activity**: Burrowing animals, such as rodents, or certain types of insects, have the potential to cause physical damage to buried cables by chewing through their insulation. This behavior exposes the conductors, which can result in an increased risk of short circuits or signal interference. In order to prevent such activity, it is often necessary to implement protective measures, such as the use of rodent-resistant cable designs.

- **Vibration from nearby infrastructure**: Cables situated in close proximity to operational infrastructure, such as railways or industrial facilities, are susceptible to persistent ground vibrations. These vibrations, generated by heavy machinery or train movements, can potentially compromise the structural integrity of the cable over time by inducing mechanical stress. Prolonged exposure to such vibrations may result in the loosening of joints, insulation damage, or even fractures in the cable.

- **Plant root growth**: The expansion of tree roots and other large plants in the vicinity of buried cables can result in mechanical pressure being exerted on the cable. Roots may encircle or penetrate the cable, causing damage to its sheath and insulation. Over time, this stress can lead to ruptures or deformation, which may compromise the cable's operational performance.

- **Crushing and puncture damage**: Cables that are buried directly in the ground are susceptible to damage from heavy objects or equipment that is operating on the surface. Compression forces exerted by machinery or the weight of vehicles can deform and weaken the cable's insulation and protective layers. Similarly, sharp objects, such as excavation tools, can puncture the cable during maintenance or construction activities, resulting in permanent damage to the conductors.

The disadvantages associated with the direct burial of signaling cables can lead to the following problem [11, 36–39]:

- **Degradation of cable sheathing**: Deterioration of the outer sheath of the cable decreases its ability to protect internal components from external influences such as moisture, chemicals, and mechanical stress. Over time, this can result in the exposure of the conductors, increasing the probability of short circuits to the ground. Such failures not only diminish the system's reliability but also pose considerable safety risks, particularly in high-voltage or critical communication applications.

- **Insulation degradation between conductors**: The deterioration of the insulation material between conductors can markedly enhance crosstalk and Electromagnetic Interference (EMI). This deterioration leads to signal distortion and an increased likelihood of short circuits between adjacent conductors, which can disrupt data transmission and compromise the system's overall functionality. It is of paramount importance to detect and replace degraded insulation at the earliest opportunity to maintain performance.

- **Conductors breakage**: The physical breakage of conductors, caused by mechanical stress, corrosion, or material fatigue, results in a complete loss of electrical continuity. This failure causes total communication disruption and can severely impact signaling operations in critical systems, such as railways or industrial automation. Therefore, it is essential to implement effective monitoring and preventive maintenance procedures to mitigate the risks of conductor breakage.

A critical aspect of these problems is their progressive severity over time, making it crucial to determine the location of cable degradation for prompt repairs accurately. For instance, Fig. 5 shows workers digging a trench to locate the specific degradation site. Repair processes can be effectively expedited if the condition of the buried multiconductor cables used by the railway signaling system is consistently monitored and documented, enabling faster intervention by a railway company's maintenance team.

To develop a monitoring solution capable of continuously informing about the physical conditions of multiconductor cables, it is necessary to devise suitable modeling and measurement methods and carry out numerical simulations and measurement campaigns. Providing a dynamic characterization of these multiconductor cables, the numerical simulations and measurement campaigns offer the conditions for extracting a set of features, from which the health of multiconductor cables can be inferred using a low-cost and less complex solution. According to the literature, the MTL theory is considered the most suitable for modeling multiconductor cables [24, 29, 40, 41]. In this sense, the following research questions are addressed in this study:

- *Is it possible to obtain a good agreement between the numerical results obtained from the MTL-based model and measurements? How do scattering parameters, NEXT and FEXT frequency responses, and characteristic impedance behave in the frequency domain?*
- *How is the propagation of electric signals through these multiconductor cables and the power spectral density (PSD) of the additive noise? Is it possible to observe channel gains that allow us to transmit low-power electric signals through these cables if we are interested in using them for data and sensing purposes?*

Figura 5 – Workers digging to repair railway signaling cables

Chapter 3 focuses on the experimental setups designed to subsidize technical answers for the posed research questions.

3 MEASUREMENT SETUP

This chapter details the configuration of three different experimental setups used to assess the behavior of a L_{ca}-length multiconductor named WirexControl V70P BFTC-1 kV, see detailed specification in datasheet [28], and widely employed in Brazilian railway signaling systems. This multiconductor cable is constituted by 12 conductors and, with a total diameter of $D = 18.5$ mm, each conductor with a diameter of $d = 1.5$ mm. The experimental setup #1 is exclusively dedicated to measuring the characteristic impedance of the multiconductor cable, thereby ensuring an accurate understanding of its electrical properties. The experimental setup #2 focuses on characterizing the $n = 1$ wire in multiconductor cable using scattering parameters, providing information on a its reflection and transmission properties. Lastly, the experimental setup #3 is designed to inject and capture voltage and current measurements in the time domain, offering a comprehensive analysis of the signal propagation behavior through conductors in the multiconductor cable.

This chapter is organized as follows: Section 3.1 details the experimental setup #1 for measuring the characteristic impedance, Section 3.2 focuses on the evaluation of the scattering parameters with experimental setup #2, and Section 3.3 covers the voltage and current measurements in the time domain with experimental setup #3.

3.1 EXPERIMENTAL SETUP #1

The experimental setup #1 is used to measure the characteristic impedance of a single conductor in a multiconductor cable. As depicted in Fig. 6, it employs a dedicated impedance measuring instrument, namely LCR meter, which is used to measure the inductance, capacitance, and resistance of passive components. A multiconductor cable segment of L_{ca} m is used to estimate the characteristic impedance. The value of the characteristic impedance for this conductor segment is given by $Z_{ca,0} = \sqrt{Z_{oc}Z_{sc}}$ [42], in which Z_{oc} and Z_{sc} are called open-circuit impedance and short-circuit impedance. The open-circuit impedance measurement is conducted by connecting the terminals of a pair of conductors to an LCR meter while leaving the opposite terminals open, allowing the LCR meter to estimate Z_{oc}. The short-circuit impedance measurement is performed by shorting the terminals on the opposite side while using the LCR meter to estimate Z_{sc}. We also used the experimental setup #1 to estimate propagation constant (γ). Consequently, we estimate $\mathbf{S}_0$ given by (2.11). Additional details about how to measure the characteristic impedance and the propagation constant for a cable and their implications for cable performance are discussed in Appendix A.

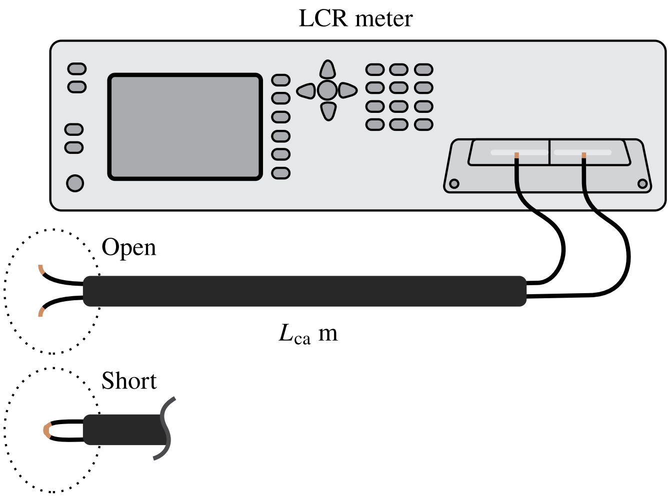

Figura 6 – An illustration of the experimental setup #1 for measuring the characteristic impedance and propagation constant in a conductor of a multiconductor cable.

3.2 EXPERIMENTAL SETUP #2

Building upon the theoretical framework presented in Section 2, the behavior between two conductors in a multiconductor cable can be analyzed by concatenating shorter segments, allowing its characterization in terms of the transmission matrix parameters $\mathbf{A}_{K-1}$, $\mathbf{B}_{K-1}$, $\mathbf{C}_{K-1}$, and $\mathbf{D}_{K-1}$. For this experiment, we consider a segment of $L_{ca} = 1$ m. To do so, we considered the experimental setup #2, illustrated in Fig. 7, to characterize a conductor in a multiconductor cable concerning its scattering parameters ($S_{0,11}$, $S_{0,12}$, $S_{0,21}$, and $S_{0,22}$), as well as NEXT and FEXT frequency responses. We obtain the direct frequency response based on the knowledge of $S_{0,12}$ or $S_{0,21}$ as we ensured that the impedance of the connected devices at both ends of the conductor is 50 Ω. The experimental setup #2 considers a segment of the multiconductor cable, designated as device under test (DUT), as illustrated in Fig 7. The multiconductor is straight and uniformly positioned above a common reference plane. A vector network analyser (VNA), powered by a line impedance stabilization network (LISN) device, measures scattering parameters, NEXT, and FEXT frequency responses of the DUT, with all other port terminated (i.e., connected to a 50 Ω load reference grounded). The use of LISN ensures minimal interference from electric power grid disturbances, effectively reducing unwanted noise during measurements. Note that the NEXT is measured when one port of the VNA is connected to the termination of one conductor and the other port is connected to the termination of a different conductor on the **same side** of the cable. In contrast, the FEXT is measured when one port of the VNA is connected to the termination of one conductor and the other port is connected to the termination of a different conductor on the **opposite side** of the cable. NEXT and FEXT, which are two types of crosstalk, are obtained from $S_{0,12}$ or $S_{0,21}$.

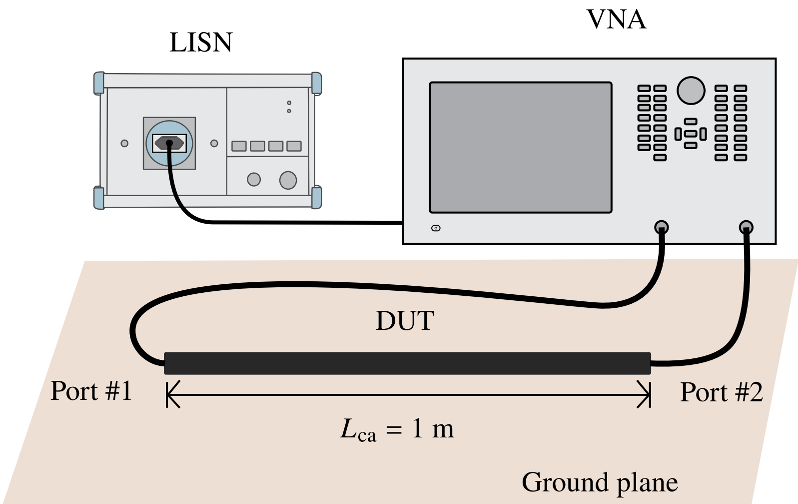

Figura 7 – An illustration of the experimental setup #2 for measuring scattering parameters, NEXT and FEXT frequency responses of a conductor of a multiconductor cable.

3.3 EXPERIMENTAL SETUP #3

The experimental setup #3 is designed to measure the signal attenuation and the PSD of additive noise in a conductor of a multiconductor cable of length L_{ca}, both in a laboratory setting and in the field. Based on the electric signals obtained from both terminals, the measurements account for a cable length of L_{ca} m and a frequency range from f_{lower} to f_{upper} MHz. Applying the Fourier transform to the measured electric signals provides estimates of the magnitude of the frequency response. The experimental setup #3 is divided into two sections, transmitter (Tx) and receiver (Rx), as shown in Fig. 8. The Tx section comprises an arbitrary waveform generator and an oscilloscope connected to the signal conditioning unit (SCU), which is in turn connected to three distinct conductors of the cable. The waveform generator produces test signals, the oscilloscope monitors the conformity of the generated test signals, and the SCU conditions and distributes these signals across three distinct conductors at one end of the multiconductor cable. At the opposite end of the multiconductor cable, the Rx section consists of SCU, which conditions the sensed test signal, and an oscilloscope, which monitors and stores the the test signal sensed by three conductors of the L_{ca}-length multiconductor cable.

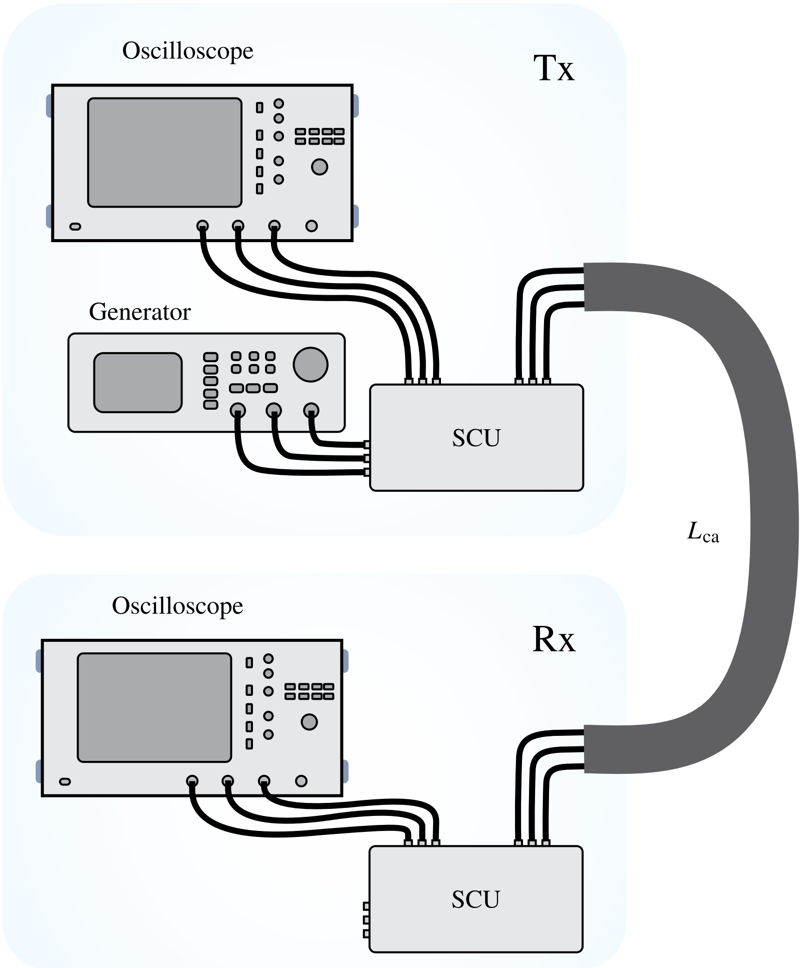

Figura 8 – An illustration of the experimental setup #3 for measuring the signal propagation and additive noise in a conductor of a multiconductor cable.

The SCU appropriately conditions both the injected electric signals into the conductor and the extracted signals from the conductor, ensuring accurate measurements. In addition, a proper grounding technique is implemented to shield the multiconductor cable. The circuit schematic of the SCU is shown in Fig. 9, and the parameters of its components are detailed in Table 2. Note that the SCU fulfills the following requirements and specifications:

- The SCU supports up to three conductor channels operating in parallel at the same printed circuit board (PCB), allowing simultaneous voltage and current measurements in the multiconductor cable. A virtual ground mimics a balanced three-phase system by injecting three sinusoidal signals generated by the arbitrary waveform with equal amplitude but with a phase shift of 120°. This configuration setup reduces interference during measurements.
- The current is measured using a shunt resistor (R7), which generates a voltage drop proportional to the current flow. This voltage signal is then amplified by the LM358 integrated circuit (CI) [43] circuit to ensure accurate readings. The amplified voltage levels are accessible via the designated bayonet neill–concelman (BNC) port for current measurement ($i(t)$). Furthermore, the cable voltage is monitored through separate BNC ports ($v(t)$ and $v_g(t)$), allowing direct observation of the cable voltage or the input voltage generation.
- The SCU employs a high-pass filter, composed of resistors (R9) and capacitor (C2), with a cutoff frequency of 93 Hz, experimentally obtained using the experimental setup #3 showed in Fig. 8. This analog filters out direct current (DC) components, allowing only the alternating current (AC) signals to be transmitted for accurate analysis. This ensures precise measurements by eliminating potential DC offsets provided by the track circuit.
- The SCU incorporates surge protection devices (SPD) to safeguard the circuit against power surges, overvoltage, and overcurrent conditions. Zener diodes (D1 to D4), arranged in a clamping configuration, limit the voltage across the conductor input by shunting excessive transient voltages to ground whenever the voltage exceeds the Zener breakdown threshold. This ensures overvoltage protection for

the sensitive measurement circuitry. Additionally, fuse (F1), rated at 100 mA, provides overcurrent protection by interrupting the current path in the event of excessive current flow, thereby preventing potential damage to the SCU.

Lastly, the 3D design and prototype of the SCU with dimensions 90 × 70 mm are shown in Fig. 10.

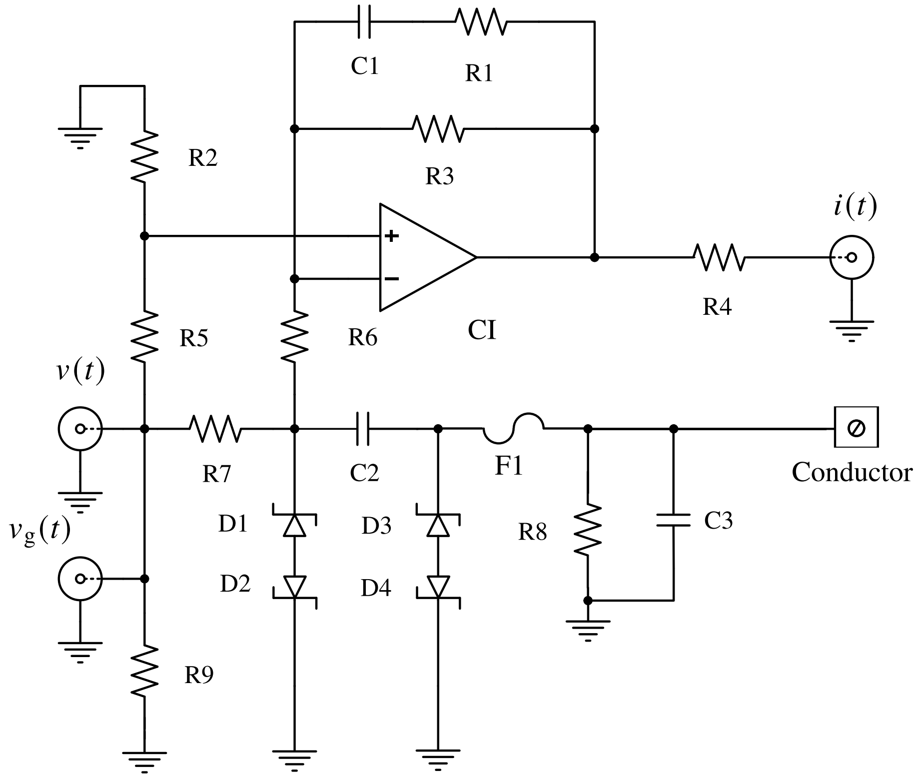

Figura 9 – The circuit schematic for the SCU.

Chapter 4 details the measurement campaign carried out in laboratory and field environments.

Component	Value
C1	1 uF
C2	17 μF
C3	1 pF
D1 and D2	13 V
D3 and D4	3.6 V
R1, R2, and R3	90.9 kΩ
R4	0 kΩ
R5 and R6	348 kΩ
R7	1 Ω
R8	100 kΩ
R9	100 Ω
F1	100 mA
CI	LM358

Tabela 2 – Information about the components used in the SCU.

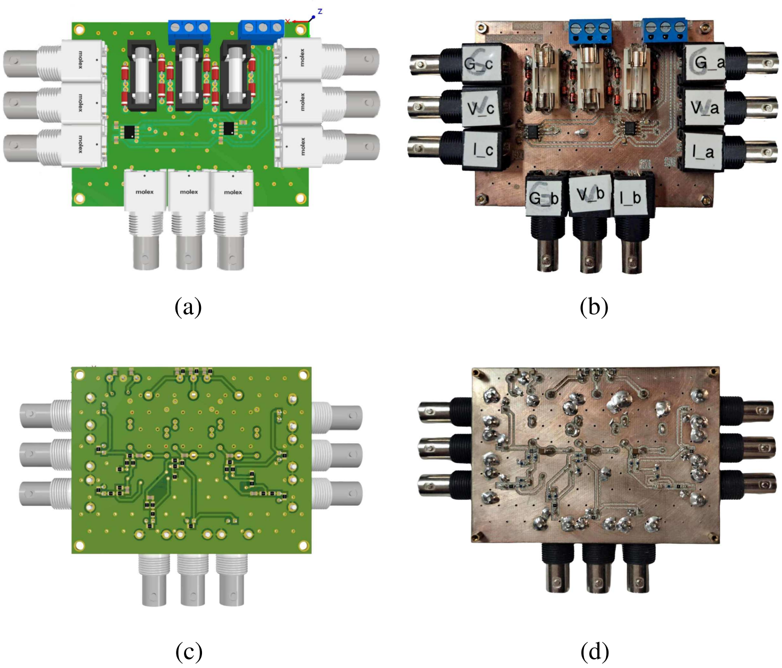

Figura 10 – Top and bottom views of the 3D design and prototype of the SCU (dimension 90×70 mm). (a) Top layer view of the 3D design. (b) Top layer view of the prototype. (c) Bottom layer view of the 3D design. (d) Bottom layer view of the prototype.

4 MEASUREMENT CAMPAIGN

This chapter describes a two-stage measurement campaign to investigate the behavior of a conductor in a multiconductor cable. The first stage was conducted in the Communications Laboratory (LCom) at Federal University of Juiz de Fora (UFJF) to validate the technical feasibility and accuracy of the experimental setups #1, #2, and #3, see Subsection 4.1. In the second stage, detailed in Subsection 4.2, a measurement campaign based on the experimental setup #3 was carried out in a segment of the railway signaling system owned by MRS Logistica S.A., in Juiz de Fora city, Minas Gerais state, Brazil. Moreover, $f_{\text{lower}} = 20$ Hz and $f_{\text{higher}} = 2$ MHz. The value of the lower-frequency edge is due to the limitations of the used equipment, while the value of the upper-frequency edge is chosen because the purpose is to characterize the multiconductor cable up to 2 MHz.

This chapter is organized as follows: Section 4.1 describes the laboratory measurement campaign, detailing the methodologies, setups, and instruments used to characterize the multiconductor cable under controlled conditions. Section 4.2 outlines the field measurement campaign conducted in a railway company site.

4.1 LABORATORY CAMPAIGN

To carry out the measurement campaign in the LCom, an $L_{\text{ca}} = 10^3$ m segment (i.e., $\Delta z = 1$ m and $k = 10^3$) of the multiconductor cable was extended across the UFJF campus, with its ends remaining inside the LCom. The cable was supplied as a spool that complies with the Brazilian standards for transport and cable spooling [44–46], as illustrated in Fig. 11. Using the experimental setup #1, estimates of the characteristic impedance were measured with the LCR meter E4980A from Keysight [42], as illustrated in Fig. 12, in the frequency range from f_{lower} Hz up to f_{upper} Hz, with the equipment set to measure 201 points.

In the sequel, the experimental setup #3 was applied to measure electrical signals at the ends of the $L_{\text{ca}} = 10^3$ m segment (i.e., $\Delta z = 1$ m and $k = 10^3$) of the multiconductor cable, as shown in Fig. 12. The three conductors located in the center of the multiconductor cable were used. In the Tx section, three arbitrary waveform generators

Figura 11 – The multiconductor spool with 1000 m used in the laboratory measurement campaign.

FY8300S [47] inject 120^o phase-shifted sinusoidal signals into the three conductors, and three Agilent DSO-X 2002A oscilloscopes [48] monitor the voltage and current signals injected into the three conductors. In the Rx section, a four-channel R&S RTE1204 [49] oscilloscope and a two-channel R&S RTH1002 [50] oscilloscope are deployed to capture the waveforms of voltage and current signals. Moreover, the SCUs in both Tx and Rx blocks are individually powered by a symmetrical 12 V_{DC} power supply.

Lastly, the experimental setup #2 was used to measure some quantities of an $L_{ca} = 1$ m segment (i.e., $\Delta z = 1$ m and $K = 1$) of the multiconductor cable, which is placed on a reference ground plane surface and connected to the VNA, as shown in Fig. 13. The VNA used is the Agilent E5061B [51], calibrated to measure in the frequency range between f_{lower} Hz and f_{upper} Hz. The VNA was power supplied by the

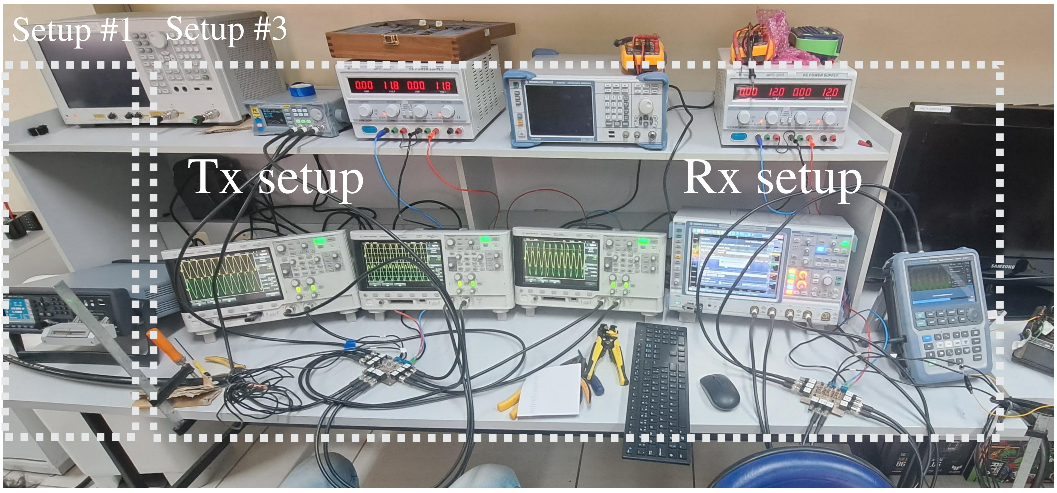

Figura 12 – Photo of the experimental setups #1 and #3 in the laboratory facility.

LISN ENV216 from R&S [52] to prevent noise from the mains network from interfering with the crosstalk measurements. When the VNA ports are connected to the same conductor, which is a reciprocal network, the measurement of the magnitude of $S_{0,21}$ or $S_{0,12}$ scattering parameter represents estimates of the direct frequency responses of a L_{ca}-length segment of a conductor in the multiconductor cable. The NEXT crosstalk is measured by connecting the VNA ports to different conductors on the same side and matching a 50 Ω termination. In contrast, the FEXT crosstalk is estimated by connecting it to conductors on opposite sides. For comparison purposes, a digital twin of measurement setup #2 was implemented and simulated in the CST Studio Suite software [53], which incorporates the MTL theory equations within a framework for cable simulation.

4.2 FIELD MEASUREMENT CAMPAIGN

The field measurement campaign was conducted in the railway signaling system of MRS Logística S.A. in Juiz de Fora, Minas Gerais, Brazil. This campaign assessed the influence of the soil because the multiconductor cable is installed underground along the edge of the railway line. This measurement campaign enables us to verify the feasibility of monitoring multiconductor cable degradation by injecting electrical signals without interfering with the railway signaling system's operation. In this sense, the measurement campaign was carried out under typical operational conditions in a

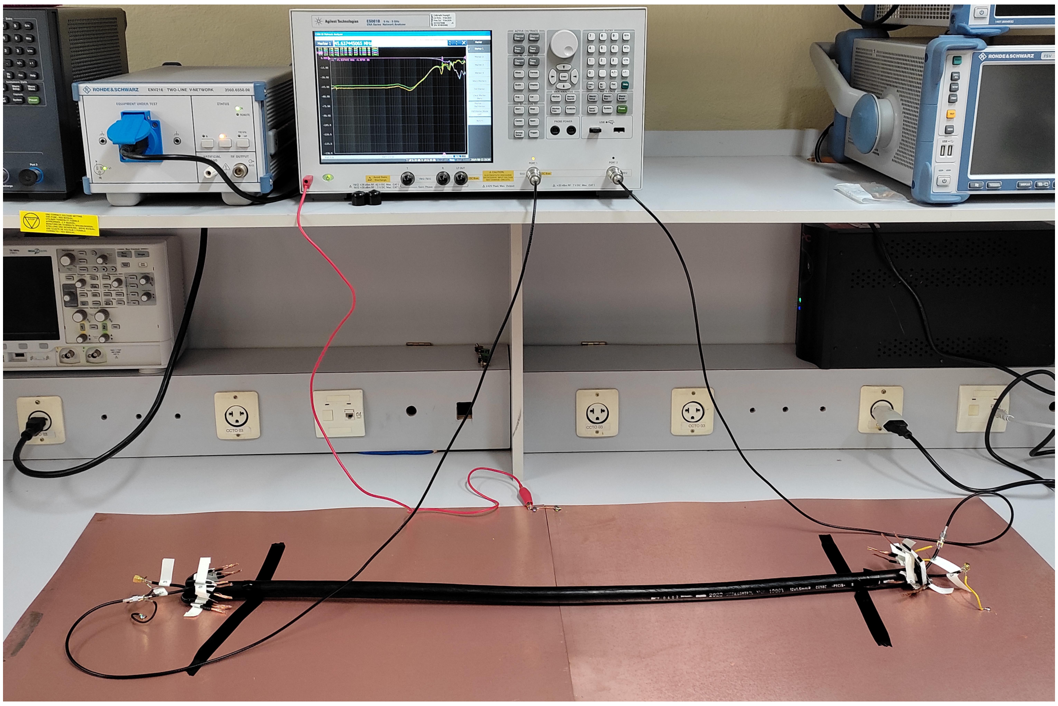

Figura 13 – Photo of the experimental setup #2 in the laboratory facility.

railway (e.g., with and without the train and wagon composition passing through the segment) when the experimental setups #1 and #3 were used. Fig. 14 shows three photos of the field measurement campaign. Note that the considered distance between the Tx and Rx devices is $L_{ac} = 1.150$ m (i.e., $\Delta z = 1$ m and $K = 1.150$) because it refers to the distance between two cabinets with railway signaling equipment in a real railway, and the multiconductor cables are applied to connect them. This distance is slightly more extended than the length considered in the measurement campaign at the laboratory facility. The injection of electric signals based on the experimental setup #3 applied to estimate the frequency response considered 21 sinusoidal signals with frequencies that are logarithmically spaced in the frequency range between f_{lower} Hz and f_{upper} Hz. In the sequel, an interpolation technique is applied to estimate the magnitude of the direct frequency response based on the information obtained by injecting 21 electric signals with sinusoidal waveforms and exponentially increasing frequencies.

Chapter 5 presents an analysis and discussion of the data collected in the laboratory and in the field.

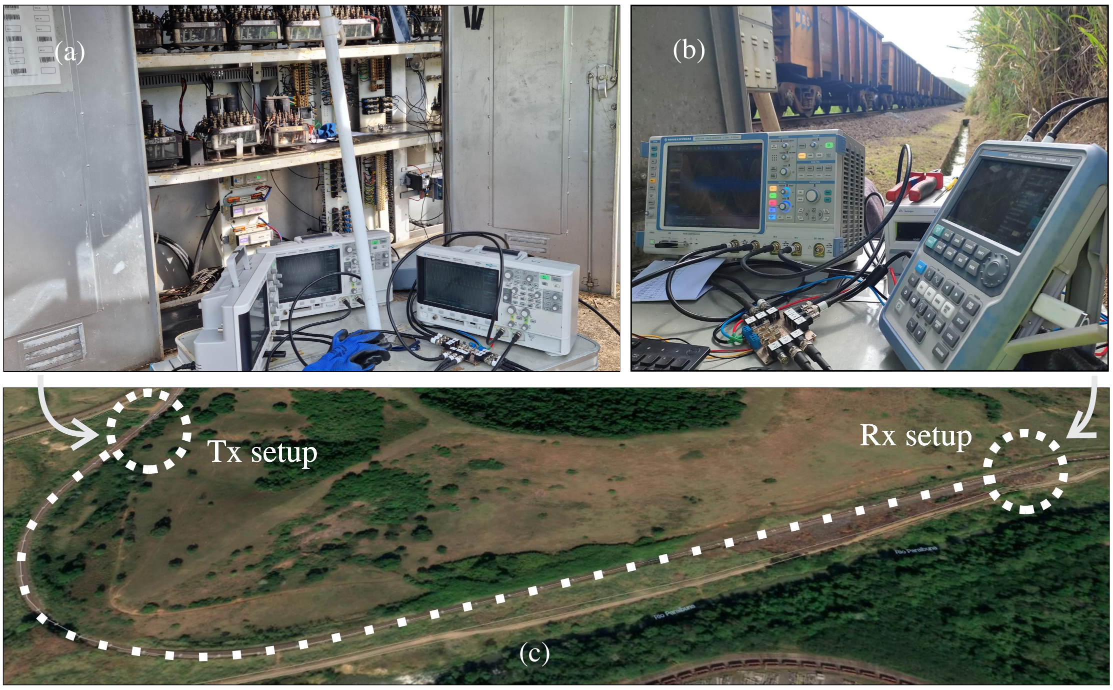

Figura 14 – Photos of the experimental setup #3 used in the field. The railway signaling system belonging to MRS Logística S.A. (a) Tx section, (b) Rx section, and (c) a segment of the railway signaling systems in Juiz de Fora city.

5 NUMERICAL RESULTS

This chapter presents the numerical results obtained with the experimental setups. All results from numerical simulation were obtained using the framework for cable simulation present in CST Studio Suite, where the electric parameters of the multiconductor cable, measured with an LCR meter, were used as inputs. Accordingly, Subsections 5.2, 5.1, and 5.3 present the results obtained with experimental setups #1, #2, and #3, respectively. For all numerical simulation and measurement campaigns, the adopted frequencies are $f_{\text{lower}} = 20$ Hz and $f_{\text{upper}} = 2$ MHz, in agreement with Section 4.

This chapter is organized as follows: Section 5.1 presents the characteristic impedance results obtained with setup #1. Section 5.2 focuses on the scattering parameters and crosstalk analysis using setup #2. Section 5.3 details the transfer function and additive noise analysis using setup #3. Finally, the section 5.4 summarizes the main findings and insights derived from the simulations and measurement campaigns.

5.1 NUMERICAL RESULTS WITH SETUP #1

Fig. 15 illustrates the magnitude and phase of the characteristic impedance obtained through numerical simulations performed using CST Studio Suite software, as well as from measurement campaigns conducted in the Communications Laboratory at UFJF (LCom) and in the field (a railway yard). The measurement results from both the LCom and field environments were acquired using an experimental setup #1.

The magnitudes of the characteristic impedance obtained in the measurement campaigns in the LCom and field, as shown in Fig. 15(a), agree across the entire frequency band, something that cannot be stated for the simulation results. Specifically, for frequencies below 1 kHz, the difference between the magnitudes of the simulation and measurement results increases as the frequency approaches f_{lower} Hz. Such a difference is due to a high-pass analog filter, which blocks the DC signal used by the railway signaling system. In contrast, the simulation and measurement magnitude results align for frequencies above 1 kHz. Moreover, the magnitudes of both simulation and measurement results converge to 85 Ω for frequencies above 1kHz. Furthermore, a zoomed-in view illustrated in Fig. 15(a) shows a slight variation around 85 Ω.

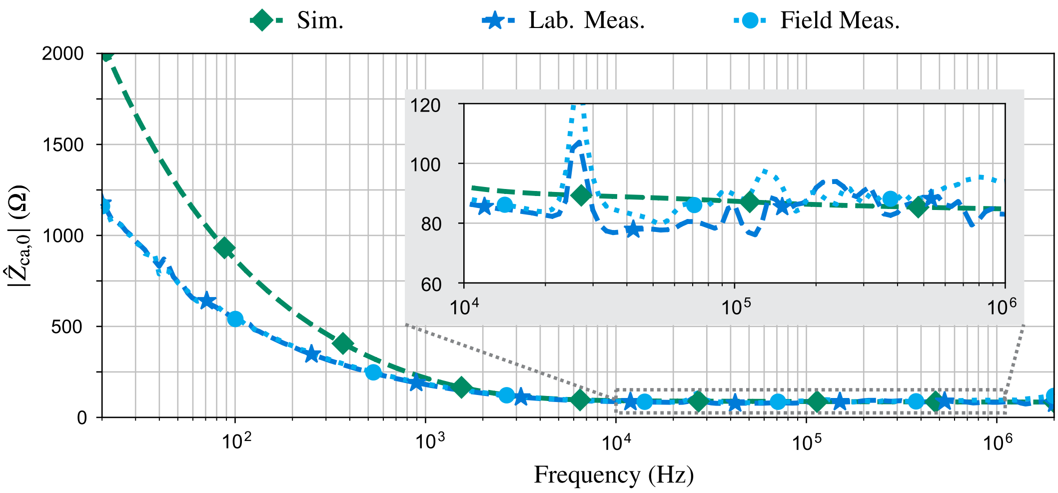

(a)

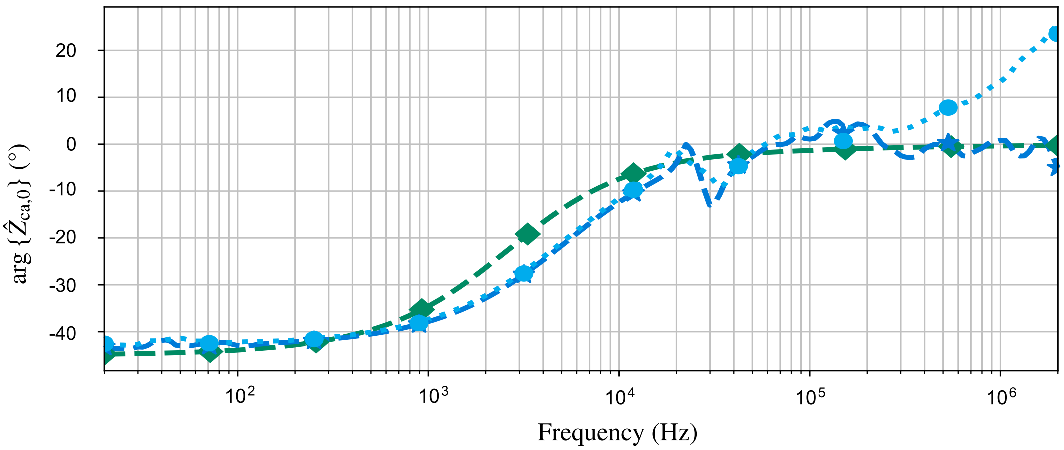

(b)

Figura 15 – Comparison of the characteristic impedance of a conductor in the multiconductor cable, obtained from numerical simulation and laboratory measurement.

Analyzing the phase of the characteristic impedance values, the curves in Fig. 15(b) show the results obtained with numerical simulations and measurements in the LCom and field. Note that the simulation and measurement results agree for the frequencies between f_{lower} Hz and 1 kHz and differ between 1 kHz and 100 kHz. Also, the simulation and LCom measurement results agree for the frequencies from 100 kHz up to f_{upper}. The phase of the characteristic impedance in Fig. 15(b) shows a predominantly capacitive behavior below 1 kHz, with values close to –40°. As frequency increases from 1 kHz to 100 kHz, the phase progressively rises toward 0°, indicating a transition to resistive behavior. Above 100 kHz, the phase becomes positive, reaching up to +20°, consistent with the presence of inductive loads in the railway signaling line, which becomes more significant at higher frequencies. These trends are consistently observed in both simulation and measurement data, though some dispersion is noticeable in field measurements beyond 300 kHz.

5.2 NUMERICAL RESULTS WITH SETUP #2

The simulation and measurement results of the magnitude of scattering parameters $S_{0,11}$and $S_{0,21}$ ($|S_{0,11}|$ and $|S_{0,21}|$) between two conductors of the multiconductor cable are shown in Fig. 16 when $L_{\text{ca}} = 1$ m and the frequency bandwidth is between f_{lower} Hz and f_{upper} Hz. The magnitude of scattering parameters $S_{0,11}$ is below -30 dB up to 1 MHz in most frequencies. The comparative analysis of the magnitude of the scattering parameter $S_{0,11}$ shows a difference of $\approx$ 6 dB between the simulation and measurement results. Additionally, measurement results indicate some randomness in frequencies up to 500 Hz, generated by the VNA, suggesting that the presence of the LISN does not eliminate the inference from the electric power grid. Overall, there is a reasonable agreement between the simulation and measurement results. Furthermore, the comparative analysis between simulation and measurement results of the magnitude of the scattering parameter $S_{0,21}$ shows excellent agreement with a slight difference for frequencies above 300 kHz. In addition, the magnitude curves of the scattering parameter curve $S_{0,21}$ provided by the simulation and measurement results confirm that the signal attenuation is irrelevant for frequencies up to f_{upper} Hz.

To analyze the crosstalk between the conductors, Fig. 17 shows the FEXT and NEXT results obtained with simulation and measurement FEXT and NEXT. Note that the FEXT crosstalk is a few dB lower than the NEXT, and both exponentially increase as the frequency increases. In addition, there is good agreement between the measurement and simulation results when the frequency is over 10 kHz. Moreover, the noise floor of the VNA imposes an increasing difference between the measurement and simulation results when the considered frequency is lower than 10 kHz because the level of these crosstalks becomes lower than the noise floor of the VNA. Moreover, as the frequency exceeds 1 MHz, both types of crosstalk become significantly more relevant, and the influence of the additive noise becomes negligible.

We noted that a L_{ca} = 1 m conductor in a multiconductor cable offers a solid characterization for modeling and performing numerical simulations based on the MTL theory in the CST Studio Suite software. In most cases, there is excellent agreement between the results obtained from the numerical simulations and the measurement campaigns. We also noted that the discrepancies between numerical simulations and measurement campaigns are mainly attributed to precautionary measures implemented in the measurement setup to avoid interference with the legacy railway signaling system.

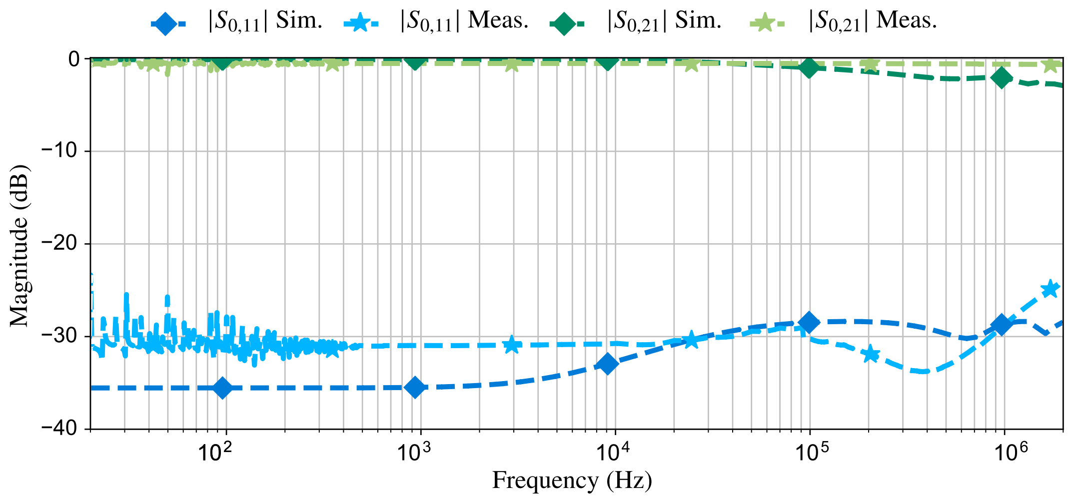

Figura 16 – Comparison between numerical results obtained from simulation and measurement in the laboratory facility for the magnitudes of the scattering parameters: $S_{0,11}$, $S_{0,12}$, $S_{0,21}$, and $S_{0,22}$.

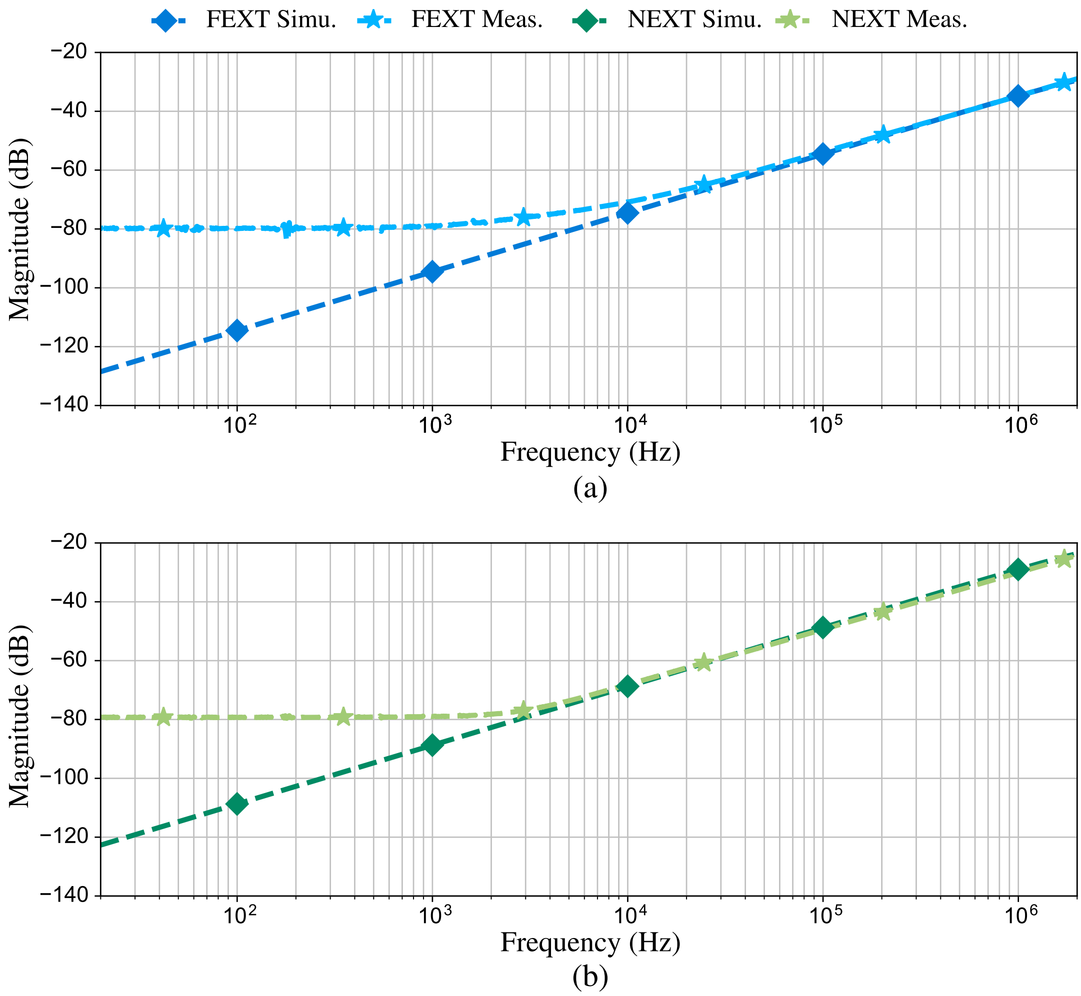

Figura 17 – Comparison between crosstalk magnitudes obtained from simulation and laboratory measurements: (a) FEXT and (b) NEXT.

5.3 NUMERICAL RESULTS WITH SETUP #3

The results obtained from the numerical simulations, as well as from the measurement campaigns conducted in the LCom and field using the experimental setup #3, for the magnitude of the direct frequency response of the $L_{ca} = 1,000$ m conductor in the multiconductor cable, are shown in Fig. 18. The magnitudes of the direct frequency responses associated with the measurement campaigns were obtained by averaging consecutive estimates of the magnitude to reduce noise in the measurement. Note that the measurement results obtained in the LCom and field differ slightly in the frequency range between 300 kHz and f_{upper} Hz. Regarding the simulation results, for frequencies between f_{lower} Hz and 100 Hz, the difference from the measurement results reduces to 0 dB. Note that the difference in 10 dB at f_{lower} Hz is due to the presence of a high-pass analog filter in the experimental setup #3, which filters out or blocks the DC signal from the railway signaling system, thereby reducing interference with the legacy system. Overall, attenuation at higher frequencies is attributed to the inherent low-pass nature of the multiconductor cable, resulting in increased attenuation as the frequency increases. Attenuation lower than 3 dB is observed when the frequency is below 100 kHz.

Considering the frequency bandwidth of $B = 100$ kHz, the length of multiconductor cables used in railway signaling systems is between 1 km and 3 km, and the copper is used in the conductors ($\epsilon_r = 2.25$), then the spatial resolution of TDR and frequency-domain reflectometry (FDR) for localizing faults is

$$\begin{aligned}\Delta d &= \frac{c}{2B\sqrt{\epsilon_r}} \\ &= 1 \text{ km}, \end{aligned} \tag{5.1}$$

In which c is the speed of light. The accurate characterization of multiconductor cables carried out in this thesis shows that neither TDR nor FDR is practical for detecting their degradation. For example, to achieve a spatial resolution better than 10 m ($\Delta d \leq 10$ m), which is a target set by the railway company to expedite maintenance once a cable fault is detected, would require a bandwidth of at least $B \geq 10$ MHz, which may not be technically feasible when the results shown in Fig. 18 is considered because a remarkable part of the spectrum for $f > 100$ kHz of the sensing signal used by TDR and FDR will be severely attenuation by the conductor. Note that for the frequencies beyond $f > 100$ kHz the PSD of the additive noise also reduces similar to the attenuation and, consequently, the use of sofisticated hardware is demanded for dealing with with signal with a very-low power.

Figure 19 shows the PSD of the additive noise measured in the field. The PSD was estimated using the Welch method[54]. In the frequency range between f_{lower} Hz and 100 kHz, the PSD reaches levels around -80 dBmV^2/Hz. This elevated PSD is attributed to the railway signaling system, which operates with DC signals. As frequency increases, the magnitude of the PSD drops significantly, reaching an average value of

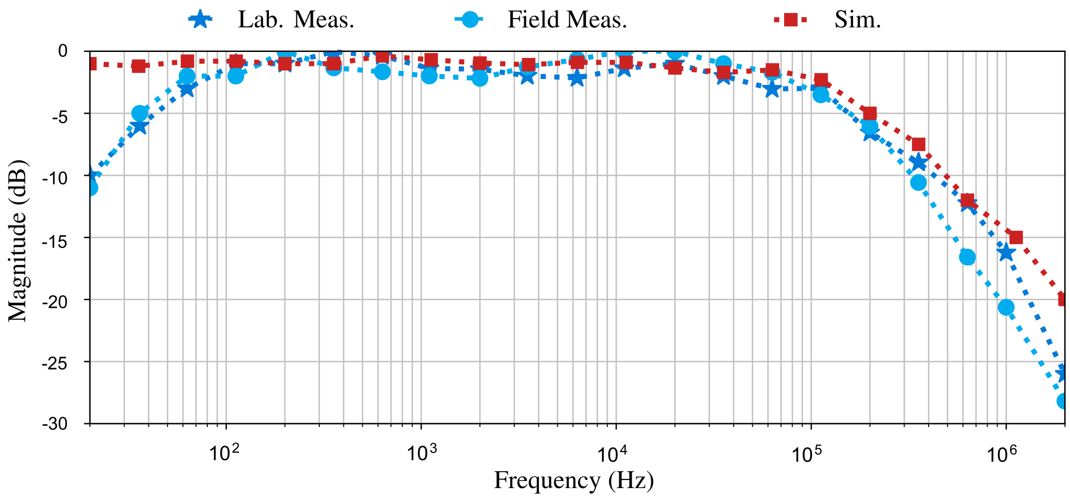

Figura 18 – Magnitude of the direct frequency response of a conductor: comparison between numerical results obtained through simulation and measurements conducted in the laboratory facility and in the field.

approximately -105 dBmV^2/Hz. In other words, a low-power electric signal can be used for both sensing and data communication.

Measurement campaigns conducted along a $L_{ca} = 10^3$ m segment of the multi-conductor cable indicate that the channel gain exceeds 105 dB across the entire frequency band. When combined with the low PSD levels of the additive noise, these results support the conclusion that low-power electric signals can be effectively employed for both data communication and sensing applications. For instance, let's consider a frequency bandwidth of $B \approx 100$ kHz, a transmitted signal power of 23 dBmW, and a frequency response attenuation of 2 dB, and PSD of the additive noise equal to -80 dBmV^2/Hz. The signal-to-noise ratio is ≈ 51 dB, which is interesting for cable sensing. Moreover, the achievable data rate is equal to ≈ 1.69 Mbps, which is useful as a secondary data communication channel for railway signaling systems because the achievable data rate is more than enough for railway signaling demands, and the use of low transmission power results in irrelevant interference with legacy railway signaling systems. Note that the frequency over $f > 100$ kHz can also be used for data communication purpose because the attenuation and the PSD of the additive noise reduces; however, it will demand more elaborate hardware to deal with the reception of low-power signals.

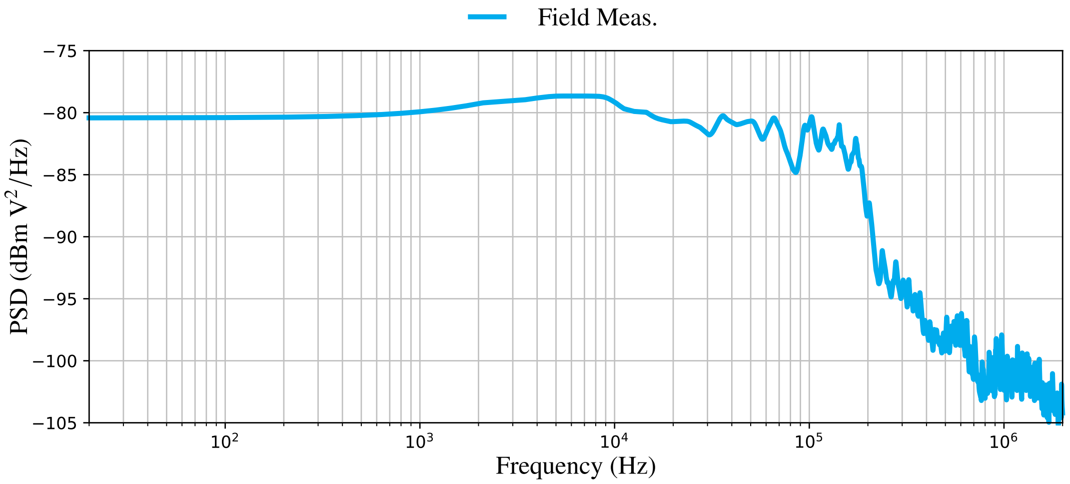

Figura 19 – An estimate of the PSD of the measured additive noise in the field.

5.4 GENERAL COMMENTS

First of all, the MTL theory in the frequency domain can effectively model the multiconductor cables used in railway signaling systems, provided the cable parameters are accurately extracted and applied in the model. The detailed experimental setups are also instrumental in carrying out measurement campaigns in laboratory and field environments.

For the frequency range between 20 Hz and 2 MHz, in most cases, there is excellent agreement between the results obtained from numerical simulations and those from measurement campaigns. When discrepancies arise between the results from numerical simulations and measurement campaigns, they primarily stem from the need to design experimental setups that do not interfere with legacy systems (i.e., the railway signaling system) and from interference originating in the railway signaling system itself.

Overall, the results from both numerical simulations and measurement campaigns showed the feasibility of using low-power electrical signals for sensing physical degradation and supporting data communication over multiconductor cables in railway signaling systems. Furthermore, exploring the dynamics of scattering parameters, crosstalk frequency response, characteristic impedance, and additive noise represents a promising avenue for predicting the physical degradation of multiconductor cables.

The conclusion of this thesis is presented in Chapter 6.

6 CONCLUSION

This thesis has studied the measurement and characterization of multiconductor cables used in railway signaling systems in the frequency band between 20 Hz and 2 MHz. Relying on the MTL theory in the frequency domain, the multiconductor cable was modeled as n wires in parallel to derive the appropriate equations for obtaining characteristic impedance, scattering parameters, crosstalk (NEXT and FEXT) and direct channel frequency responses. Also, it discussed three simulation setups for measuring the characteristic impedance, scattering parameters, NEXT and FEXT frequency responses, and the waveform of electric signals and additive noise of a multiconductor cable in both the laboratory and the field. Moreover, it presented results related to numerical simulations performed by CST Studio Suite software and measurement campaigns based on the three experimental setups. A comparison between the results obtained from these numerical simulations and those from the measurement campaigns carried out in the laboratory and the field provided valuable insights.

The measurement campaign of the $L_{ca} = 1$ m multiconductor cable offers a solid characterization for modeling and performing numerical simulations based on the MTL theory. In most cases, there is excellent agreement between the results obtained from the numerical simulations and the measurement campaigns. Some differences arise due to constraints related to the implementation of experimental setups and limitations of the equipment used. Overall, numerical simulations relying on MTL theory are valuable for analyzing multiconductor cables in railway signaling systems, provided the cable parameters are correctly determined. Indeed, there is a strong correlation between the results from the numerical simulations and those from the measurement campaigns. Moreover, measurement campaigns using $L_{ca} = 10^3$ m show that signal attenuation is low, and the additive noise exhibits a PSD that facilitates analyzing the waveform of electric signals transmitted through the multiconductor cables for monitoring purposes.

The agreement between simulated and measured data confirm the usefulness of both modeling and experiments in laboratory and in the field for allowing the use of the CST Studio Suite software for performing numerical analysis of multiconductor cable. Furthermore, this alignment underlines its applicability to real-world railway environments and its effectiveness in delivering accurate insights into multiconductor cable performance under diverse conditions.

Considering the low level of attenuation for the frequency bandwidth between 0 and 100 kHz, this investigation concludes that in this frequency bandwidth both data communication and cable sensing can be effectively achieved using low-power electric signals and, consequently, without interference in legacy railway signaling systems. Moreover, the high level of attenuation in the signal propagation when its frequency content is over 100 kHz suggests that time- and frequency-based reflectometry techniques may not be feasible.

6.1 FUTURE WORK

Future work involves expanding the scope of the measurement campaign to encompass all conductors in the multiconductor cable and, consequently, constructing a comprehensive dataset covering faults and degradation patterns. The analysis of these dataset will allow to come up with a set of features that are really relevant for monitoring the degradation of multiconductor cables. Consequently, it will be feasible to use machine learning (ML)-based algorithms for predicting degradation and informing its type of degradation early fault detection and localization. These efforts are expected to enhance the long-term reliability and safety of railway signaling systems by allowing continuous, non-invasive assessment of multiconductor cable integrity.

REFERENCES

[1] P. R. P. Sampaio and M. T. Daychoum, "Two decades of rail regulatory reform in brazil (1996–2016)," *Utilities Policy*, vol. 49, pp. 93–103, 2017. [Online]. Available: https://www.sciencedirect.com/science/article/pii/S0957178716302594

[2] National Association of Railway Transporters (ANTF). "Railway Map."ANTF.org.br. Sep. 05, 2024. [Online.] Available: https://www.antf.org.br/mapa-ferroviario.

[3] L. S. Thompson and J. C. Kohon, "Developments in rail organization in the Americas, 1990 to present and future directions," *J. Rail Transp. Plan. Manag.*, vol. 2, no. 3, pp. 51–62, dec. 2012.

[4] Câmara Temática de Infraestrutura e Logística (CTLOG), "Apresentação CTLOG," Ministério da Agricultura, Pecuária e Abastecimento, Brasília, DF, Brasil, Set. 2024. [Online]. Disponível em: https://www.gov.br/agricultura/pt-br/assuntos/camaras-setoriais-tematicas/documentos/camaras-tematicas/infraestrutura-e-logistica/2024/97a-ro-04-09-2024/apresentacao_ctlog.pdf.

[5] Y. Wu and P. Zhang, "A novel online monitoring scheme for underground power cable insulation based on common-mode leakage current measurement," *IEEE Transactions on Industrial Electronics*, vol. 69, no. 12, pp. 13 586–13 596, Dec. 2022.

[6] Y. Wu, Y. Yang, Z. Wang, and P. Zhang, "Online monitoring for underground power cable insulation based on common-mode signal injection," *IEEE Transactions on Industrial Electronics*, vol. 69, no. 12, pp. 13 586–13 596, Dec. 2022.

[7] Y. Huo, G. Prasad, L. Lampe, and V. Leung, "Power Line Communication and sensing using time series forecasting," *Sensors*, vol. 22, no. 5320, pp. 1–19, Jul. 2022.

[8] A. Q. Gbadamosi, L. O. Oyedele, J. M. D. Delgado, H. Kusimo, L. Akanbi, O. Olawale, and N. Muhammed-yakubu, "IoT for predictive assets monitoring and maintenance: An implementation strategy for the UK rail industry," *Automation in Construction*, vol. 122, p. 103486, Feb. 2021.

[9] T. A. Alvarenga, "Identificação e localização de falhas em circuitos de via de ferrovias baseadas em reflectometria no domínio da frequência," Ph.D. dissertation, Dept. de Eng. Elétrica, Univ. Federal de Juiz de Fora, Juiz de Fora, MG, 2018.

[10] R. Bridgelall and D. D. Tolliver, "Railroad accident analysis by machine learning and natural language processing," *Journal of Rail Transport Planning and Management*, vol. 29, no. 100429, pp. 1–14, Mar. 2024.

[11] R. Vijay, G. Prasad, Y. Huo, S. Sm, and P. Tv, "Measurement-based condition monitoring of railway signaling cables," in *2021 IEEE International Conference on Communications, Control, and Computing Technologies for Smart Grids (SmartGridComm)*, Dec. 2021, pp. 33–38.

[12] R. Vijay and T. Prabhakar, "Causal ai for cable health monitoring," *Measurement*, vol. 253, p. 117705, 2025. [Online]. Available: https://www.sciencedirect.com/science/article/pii/S0263224125010644

[13] P. Smith, C. Furse, and J. Gunther, "Analysis of spread spectrum time domain reflectometry for wire fault location," *IEEE Sensors Journal*, vol. 5, no. 6, pp. 1469–1478, dec 2005.

[14] L. G. D. Oliveira, M. D. L. Filomeno, H. V. Poor, and M. V. Ribeiro, "Orthogonal chirp-division multiplexing for power line sensing via time-domain reflectometry," *IEEE Sensors Journal*, vol. 21, no. 2, pp. 955–964, Jan. 2021.

[15] L. G. de Oliveira, M. de L. Filomeno, H. V. Poor, and M. V. Ribeiro, "Fault detection and location in power distribution systems: The usefulness of the HS-OFDM scheme for time-domain reflectometry," *Electric Power Systems Research*, vol. 74, pp. 949–958, Feb. 2022.

[16] G. Prasad, Y. Huo, L. Lampe, A. Mengi, and V. C. Leung, "Fault diagnostics with legacy power line modems," in *Proceedings of the 2019 IEEE International Symposium on Power Line Communications and its Applications, ISPLC 2019*, Apr. 2019, pp. 1–6.

[17] L. Benesl, P. Mlynek, M. Ptacek, V. Vycital, J. Misurec, J. Slacik, M. Rusz, and P. Musil, "Cable monitoring using broadband power line communication," *Sensors*, vol. 22, 2022.

[18] Y. Huo, G. Prasad, L. Atanackovic, L. Lampe, and V. C. Leung, "Cable diagnostics with power line modems for smart grid monitoring," *IEEE Access*, vol. 7, pp. 60 206–60 220, Jan. 2019.

[19] D. Grzechca, D. Zieliński, and W. Filipowski, "What is the effect of outer jacket degradation on the communication parameters? a case study of the twisted pair cable applied in the railway industry," *Energies*, vol. 14, 2021.

[20] T. R. Oliveira, C. A. Marques, W. A. Finamore, S. L. Netto, and M. V. Ribeiro, “A methodology for estimating frequency responses of electric power grids,” *Journal of Control, Automation and Electrical Systems*, vol. 25, no. 6, pp. 720–731, Sep. 2014.

[21] P. Fraga-Lamas, T. M. Fernández-Caramés, and L. Castedo, “Towards the internet of smart trains: A review on industrial iot-connected railways,” *Sensors (Switzerland)*, vol. 17, 2017.

[22] M. V. Ribeiro, M. D. L. Filomeno, A. Camponogara, T. R. Oliveira, T. F. Moreira, S. Galli, and H. V. Poor, “Seamless connectivity: The power of integrating power line and wireless communications,” *IEEE Communications Surveys and Tutorials*, vol. 26, no. 1, pp. 1–40, Apr. 2024.

[23] T. Zhuang, M. Ren, X. Gao, M. Dong, W. Huang, and C. Zhang, “Insulation condition monitoring in distribution power grid via iot-based sensing network,” *IEEE Transactions on Power Delivery*, vol. 34, pp. 1706–1714, Ago. 2019.

[24] C. R. Paul, *Analysis of Multiconductor Transmission Lines*, 2nd ed. New Jersey, USA: John Wiley & Sons, 2008.

[25] *Railway signaling - Circuit track - classification*, Associação Brasileira de Normas Técnicas (ABNT) Std. NBR 8362, Sep. 2012.

[26] *Railway signaling — Eletrical power lines and eletrica lines for vital sign and not vital - Surge protective devices (SPD)*, Associação Brasileira de Normas Técnicas (ABNT) Std. NBR 13 184, Mar. 2012.

[27] *Railway signaling — Light signal with one or two light units — Signal aspect*, Associação Brasileira de Normas Técnicas (ABNT) Std. NBR 12 511, Aug. 2012.

[28] Wirex. "Control and Instrumentation Cables."wirex.com.br. July 29, 2024. [Online.] Available: www.wirex.com.br/pt-br/produtos/cabos-de-controle-e-instrumentacao.

[29] C. R. Paul, “A brief history of work in transmission lines for EMC applications,” *IEEE Transactions on Electromagnetic Compatibility*, vol. 49, no. 2, pp. 237–252, May 2007.

[30] F. Versolatto and A. M. Tonello, “An MTL theory approach for the simulation of MIMO power-line communication channels,” *IEEE Transactions on Power Delivery*, vol. 26, no. 3, pp. 1710–1717, Jul. 2011.

[31] C. R. Paul, “Useful matrix chain parameter identities for the analysis of multiconductor transmission lines,” *IEEE Transactions on Microwave Theory and Techniques*, vol. 23, no. 9, pp. 756–760, Sep. 1975.

[32] B. Lee, J. M. Cioffi, S. Jagannathan, K. Seong, Y. Kim, M. Mohseni, and M. H. Brady, “Binder MIMO channels,” *IEEE Transactions on Communications*, vol. 55, no. 8, pp. 1617–1628, Aug. 2007.

[33] R. Papazyan, P. Pettersson, H. Edin, R. Eriksson, and U. Gafvert, “Extraction of high frequency power cable characteristics from s-parameter measurements,” *IEEE Trans. Dielectr. Electr. Insul.*, vol. 11, no. 3, pp. 461–470, 2004.

[34] S. Jagannathan, V. Pourahmad, K. Seong, J. M. Cioffi, M. Ouzzif, and R. Tarafi, “Common-mode data transmission using the binder sheath in digital subscriber lines,” *IEEE Transactions on Communications*, vol. 57, no. 3, pp. 831–840, Mar. 2009.

[35] B. Lee, J. M. Cioffi, S. Jagannathan, K. Seong, Y. Kim, M. Mohseni, and M. H. Brady, “Binder MIMO channels,” *IEEE Transactions on Communications*, vol. 55, no. 8, pp. 1617–1628, 2007.

[36] Y. Li, L. Jiang, M. Xie, J. Yu, L. Qian, K. Xu, M. Chen, and Y. Wang, “Advancements and challenges in power cable laying,” *Energies*, vol. 17, no. 12, 2024.

[37] T.-P. Electrical, “Underground versus aerial cabling: Pros and cons of each,” https://tri-powerelectrical.com/underground-versus-aerial-cabling-pros-and-cons-of-each/?utm_source=chatgpt.com, 2022, accessed: July 2, 2025.

[38] ReMEE, “Why direct burial cables are important,” https://remee.com/why-direct-burial-cables-are-important/?utm_source=chatgpt.com, 2024, accessed: July 2, 2025.

[39] CableDataSheet.com, “Underground cable system,” https://www.cabledatasheet.com/pdf/Underground%20Cable%20System.pdf, accessed: July 2, 2025.

[40] B. Lee, J. M. Cioffi, S. Jagannathan, K. Seong, Y. Kim, M. Mohseni, and M. H. Brady, “Binder mimo channels,” *IEEE Transactions on Communications*, vol. 55, no. 8, pp. 1617–1628, 2007.

[41] J. A. Corchado, J. A. Cortés, F. J. Cañete, and L. Díez, “An mtl-based channel model for indoor broadband mimo power line communications,” *IEEE Journal on Selected Areas in Communications*, vol. 34, no. 7, pp. 2045–2055, 2016.

[42] Keysight Technologies, *E4980A Precision LCR Meter*, https://www.keysight.com/us/en/assets/7018-01355/data-sheets/5989-4435.pdf, Sep. 2024.

[43] Texas Instruments. LMx58-N Low-Power, Dual-Operational Amplifiers. (2022). Accessed: 13, Nov, 2024. [Online] Available: https://www.ti.com/lit/ds/symlink/lm158-n.pdf.

[44] *Cables for Electrical Installations with Extruded XLPE, EPR, or HEPR Insulation for Rated Voltages up to 1 kV - Performance Requirements*, Associação Brasileira de Normas Técnicas (ABNT) Std. NBR 7310, 2011.

[45] *Cables for Telecommunication - Specifications for Optical and Metallic Cable Construction*, Associação Brasileira de Normas Técnicas (ABNT) Std. NBR 11 137, 2017.

[46] *Cables for Instrumentation - Specification for Performance of Instrumentation and Control Cables*, Associação Brasileira de Normas Técnicas (ABNT) Std. NBR 9511, 2019.

[47] FeelTech, *Signal Generator*, dec. 2024. [Online]. Available: https://supereyes.ru/img/instructions/FY8300_manual.pdf

[48] Keysight Technologies. DSOX2002A Oscilloscope, 2 ports, 70 MHz. (2017). Accessed: 12 Dec 2024. [Online] Available: https://www.keysight.com/us/en/product/DSOX2002A/oscilloscope-70-mhz-2-analog-channels.html.

[49] Rohde & Schwarz. FSH8 Scope Rider Oscilloscope RTH1204. (2014). Accessed: 15, Dec, 2024. [Online] Available: https://www.rohde-schwarz.com/webhelp/RTH_HTML_UserManual_en/Content/welcome.htm.

[50] Rohde & Schwarz. RTH1002 Digital Oscilloscope. (2015). Accessed: 15, Dec, 2024. [Online] Available: https://www.rohde-schwarz.com/webhelp/RTH_HTML_UserManual_en/Content/welcome.htm.

[51] Agilent. E5061B Vector Network Analyzer 2 ports, 5 Hz - 3 GHz. (2009). Accessed: 15, Dec, 2024. [Online] Available: https://jahschwa.com/~kiosk/equip/agilent/e5061b/agilent-e5061b-manual.pdf.

[52] Rohde & Schwarz. ENV216 Two-line V-network. (2012). Accessed: 09, Dec, 2024. [Online] Available: https://www.rohde-schwarz.com/webhelp/ENV216_html_usermanual_en/Content/welcome.htm.

[53] CST Studio Suite. (2023). Dassault Systèmes. Accessed: 15, Dec, 2024. [Online] Available: https://www.3ds.com/products-services/simulia/products/cst-studio-suite/.

[54] P. Welch, "The use of fast fourier transform for the estimation of power spectra: A method based on time averaging over short, modified periodograms," *IEEE Trans. Audio Electroacoust.*, vol. AE-15, no. 2, pp. 70–73, Jun. 1967.

[55] B. A. Munk, *Appendix C: How to Measure the Characteristic Impedance and Attenuation of a Cable*. John Wiley & Sons, Ltd, 2009, pp. 167–173.

[56] Impedance Measurement Handbook: A guide to measurement technology and techniques, 6th ed., Keysight Technologies, Santa Rosa, CA, USA, 2020.

Appendix A – MEASUREMENT IMPEDANCE CHARACTERISTIC AND PROPAGATION CONSTANT WITH LCR METER

Determining the characteristic impedance, denoted as $Z_{\mathrm{ca},0}$, and propagation constants, represented by the γ, is a fundamental step in the evaluation of cable performance [55]. This appendix provides a methodology for measuring and obtaining these parameters with the precision LCR meter manufactured by the Keysight model E4980A [42].

The measurement process commences with the connection of the cable under examination to the high and low terminals of the test fixture. The high terminal is attached to the outer conductor of the cable, thus minimizing the effects of noise, which is a crucial consideration when testing long cable sections, as illustrated in Fig. 6. To determine the characteristic impedance and propagation constants, measurements are conducted using the open-short method. Following this procedure:

1. **Open Measurement:** The far end of the cable is left open, creating an open-circuit condition. The LCR meter measures the impedance Z_{oc} across the cable at the desired frequencies.

2. **Short Measurement:** The far end of the cable is then short-circuited, creating a closed-circuit condition. The LCR meter measures the impedance Z_{sc} in this configuration.

In light of the deduction mentioned above, the characteristic impedance $Z_{\mathrm{ca},0}$ can be expressed in terms of magnitude and phase as follows [56]:

$$Z_{\mathrm{ca},0} = \sqrt{Z_{\mathrm{oc}} Z_{\mathrm{sc}}} \quad (\Omega) \tag{A.1a}$$

$$\theta = \frac{\theta_{\mathrm{oc}} + \theta_{\mathrm{sc}}}{2} \quad (\mathrm{deg}). \tag{A.1b}$$

The propagation constant, γ, is represented in its complex form as $\gamma = \alpha + \mathrm{j}\beta$, where α is the attenuation constant and β is the phase constant. These parameters are fundamental for analyzing wave propagation in transmission lines, including multiconductor cables commonly used in railway systems. They characterize signal behavior along the cable, accounting for factors such as resistance, reactance, and cable length, denoted as L (in meters). The attenuation constant (α) and the phase constant (β) are given by [42]

$$\alpha = \frac{1}{2\mathrm{L}} \ln\left(\sqrt{\frac{(1+\mathrm{R}_k)^2 + \mathrm{X}_k^2}{(1-\mathrm{R}_k)^2 + \mathrm{X}_k^2}}\right) \times 8.6859 \qquad \text{(dB/m)} \qquad \text{(A.2a)}$$

$$\beta = \frac{1}{2\mathrm{L}} \left(\pi - \arctan\left(\frac{\mathrm{R}_k + 1}{\mathrm{X}_k}\right) + \arctan\left(\frac{\mathrm{R}_k - 1}{\mathrm{X}_k}\right)\right) \qquad \text{(rad/m)}. \qquad \text{(A.2b)}$$

The quantities R_k and X_k correspond, respectively, to the real and imaginary components of the normalized impedance ratio. Both are expressed in neper per meter (Np/m)[1] and expressed as

$$\mathrm{R}_k = \sqrt{\frac{|Z_{\mathrm{sc}}|}{|Z_{\mathrm{oc}}|}} \cos\left(\frac{\theta_{\mathrm{sc}} - \theta_{\mathrm{oc}}}{2}\right) \qquad \text{(Np/m)} \qquad \text{(A.3a)}$$

$$\mathrm{X}_k = \sqrt{\frac{|Z_{\mathrm{sc}}|}{|Z_{\mathrm{oc}}|}} \sin\left(\frac{\theta_{\mathrm{sc}} - \theta_{\mathrm{oc}}}{2}\right) \qquad \text{(Np/m)}. \qquad \text{(A.3b)}$$

[1] 1 Np = 8.6859 dB

Appendix B – PUBLICATIONS

During the master's program, the author made significant contributions to the scientific community, resulting in two conference articles, three journal articles, one book chapter, and three poster presentations.

1. The list of conference papers published during the graduate period:

    a) W. M. Cantarino, V. E. Monteiro, L. G. da S. Costa, and M. V. Ribeiro, "Passive analog blocking filter for narrowband PLC systems," *2023 Symposium on Internet of Things (SIoT)*, São Paulo, Brazil, Oct. 2023, pp. 1–5, doi: 10.1109/SIoT60039.2023.10390028.

    b) L. G. da S. Costa, T. C. Rocha, G. H. B. Goncalves, W. M. Cantarino, G. N. de S. Ribeiro, and M. V. Ribeiro, "An augmented capacitive coupling circuit for boosting PLC systems in IoT domains," *2023 Symposium on Internet of Things (SIoT)*, São Paulo, Brazil, Oct. 2023, pp. 1–5, doi: 10.1109/SIoT60039.2023.10390135.

2. The list of journal papers submitted during the graduate period:

    a) W. M. Cantarino, V. E. Monteiro, L. G. da S. Costa, G. H. B. Goncalves, G. N. de S. Ribeiro, A. M. Tonello, and M. V. Ribeiro, "Measurement and Characterization of Multiconductor Cables in Railway Signaling Systems," *IEEE Open Journal of Intelligent Transportation Systems*. Under review.

    b) M. C. de Souza, W. M. Cantarino, L. G. da S. Costa, T. A. Curty, D. A. B. Fonseca, U. R. C. Vitor, and M. E. V. Segatto, "Characterizing MIMO channels in low-voltage electric power line communication through impedance and scattering parameters analysis," *Journal of Microwaves Optoelectronics and Electromagnetic Applications*, vol. 23, no. 2, May 2024, doi: 10.1590/2179-10742024v23i3289482.

    c) D. A. B. Fonseca, L. G. da S. Costa, W. M. Cantarino, and U. R. C. Vitor, "Assessment of planar transmission line with stub for measuring water content in power transformer oil," *Journal of Microwaves, Optoelectronics and*

Electromagnetic Applications, vol. 24, no. 1, Jan 2025. doi:10.1590/2179-10742025v24i1287232.

3. The list of chapters of the book submitted during the graduate period:

    a) L. G. da S. Costa, W. M. Cantarino, G. N. de S. Ribeiro, C. M. S. Fonseca, M. de L. Filomeno, U. R. C. Vitor, and M. V. Ribeiro, "A guide to prototyping broadband and capacitive power line communication coupling circuits for low-voltage electric power grids,"in *Power Line Communication Systems for Smart Grids*, Chapter 10, pp. 283–315, The IET, 2024. doi:10.1049/PBPO260E_ch10.

4. The list of poster papers submitted during the graduate period:

    a) G. N. de S. Ribeiro, G. H. B. Gonçalves, W. M. Cantarino, V. E. Monteiro, L. G. da S. Costa, L. M. A. Filho, and M. V. Ribeiro, "A multiconductor study applied to railways," *2024 IINCEE Energy Transition*, Aug. 2024. The work received the Best Poster Award.

    b) C. M. S. Fonseca, C. M. M. Adetonah, W. M. Cantarino, V. E. Monteiro, L. G. da S. Costa, M. V. Ribeiro, M. A. O. Schroeder, and G. L. Ramos, "Analyzing design-prototype discrepancies in microstrip patch antennas for IoT applications," *2023 IoT Forum*, Oct. 2023.

    c) G. S. de Albuquerque, D. de S. da Silva, W. M. Cantarino, and E. C. Teixeira, "Fifty years of the 555 timer – a tribute from a didactic IC design perspective," *23rd Microelectronics Students Forum (SForum 2023)*, Aug. 2023.